Consortium

for

Small-Scale Modelling

Deutscher
Wetterdienst

MeteoSwiss

Ufficio Generale Spazio
Aereo e Meteorologia

EΘNIKH
METEΩPOΛOΓIKH
ΥΠHPEΣIA

Instytucie Meteorogii i
Gospodarki Wodnej

Administratia Nationala de
Meteorologie

Agenzia Regionale per la
Protezione Ambientale del
Piemonte

Agenzia Regionale per la Protezione
Ambientale dell' Emilia-Romagna:
Servizio Idro-Meteo-Clima

Centro Italiano Ricerche
Aerospaziali

Amt für GeoInformationswesen
der Bundeswehr

www.cosmo-model.org

COSMO Priority Project "Further Developments of the Runge-Kutta Time Integration Scheme (RK)": Final Report

Project participants:

M. Baldauf [‡], G. Ceci, J. Förstner, O. Fuhrer,

A. Gassmann, H-J. Herzog, G. de Morsier, T. Reinhardt,

G. Rivin, L. Torrisi, P. L. Vitagliano, G. Zängl

[‡] Project Leader:
Michael Baldauf
Deutscher Wetterdienst
Offenbach
Germany

Contents

1 Summary

The Priority Project Runge-Kutta started in October 2005 and ended after 3 years in September 2008. The starting point was an implementation of the Runge-Kutta (RK) method (Wicker and Skamarock 1998, Wicker and Skamarock 2002, Skamarock et al. 2005) into the COSMO-model at DWD beginning mid 2003 as the basic time integration scheme for use in high resolution applications. The aim was to replace the Klemp and Wilhelmson (1978) leapfrog-scheme later on. The Runge-Kutta method offers a substantial gain in accuracy at no additional costs. At the beginning of the Priority Project 10 tasks were defined (in a rather arbitrary order). During the project 4 additional tasks arose. These tasks can roughly be grouped into 3 classes:

- Repair detected model deficiencies:

    1 - Looking at pressure bias

    4 - Advection of moisture quantities in conservation form

    6 - Deep valleys

    7 - Different filter options for orography

    14 - DFI for RK

- New developments:

    8 - Higher order discretization in the vertical

    9 - Physics coupling scheme

    10 - Testing of alternative fast wave scheme

    13 - Divergence damping in a truly 3D-version

- Tool development:

    2 - Continue RK case studies

    3 - Conservation tool

    5 - Investigation of convergence

The two tasks

11 - Development of a more conservative dynamics

12 - Development of an efficient semi-implicit solver in combination with RK time integration scheme

were found to be too ambitious to be handled into this project. Indeed task 11 will evolve into an entirely new Priority Project ('Conservative Dynamical Core (CDC)').

Fortunately the tasks (1, 4, 6, 7, 14) which handle detected model deficiencies could be treated and came to a satisfactory end. This holds in particular for the rather tenacious problem of the pressure bias, task 1, which could be solved by a combination of several measures. The new moisture transport schemes are probably the main responsible for the improvements of the precipitation forecast, which were detected in the Priority Project 'Quantitative precipitation forecast' by comparing the old and new dynamical core (Leapfrog vs. RK). Also the tool development tasks (3, 5) could fulfil all the required deliverables.

The integration tool is now applied e.g. at the MPI Hamburg for budget inspections of moisture. A solver for analytic solutions for mountain flows is available, which was developed in particular for model validation. The tools for measuring the convergence rate are also available now. Task 2 had no concrete deliverables but accompanied the project by verifying the efforts of the projects by case studies and by identifying possible new problems of the dynamical core (e.g. the stability problem of thin layers near the ground). From the 'new development' tasks, task 9 is merely in an intermediate state. Task 8 (implicit vertical advection) could be brought to a satisfactory state some months after the official end of the project. At least, the necessary methodologies (needed efficient linear equation solver, model configuration items) are delivered and several studies were performed. Task 13 (3D-divergence) could not be treated at all. There was some time invested into task 10 to bring this version into a state for operational use. All in all it was found that some ideas contained there were promising, but a bigger effort is required to solve some more fundamental questions before it could be used.

2 Project report

2.1 Task 1: Looking at pressure bias

The pressure bias problem in RK core was pointed out in Torrisi (2005). Objective verification results using SYNOP observations showed a difference in mean sea-level pressure (MSLP) bias behaviour between 7 km Runge Kutta (RK) and LeapFrog (LF) runs (Fig. 1)
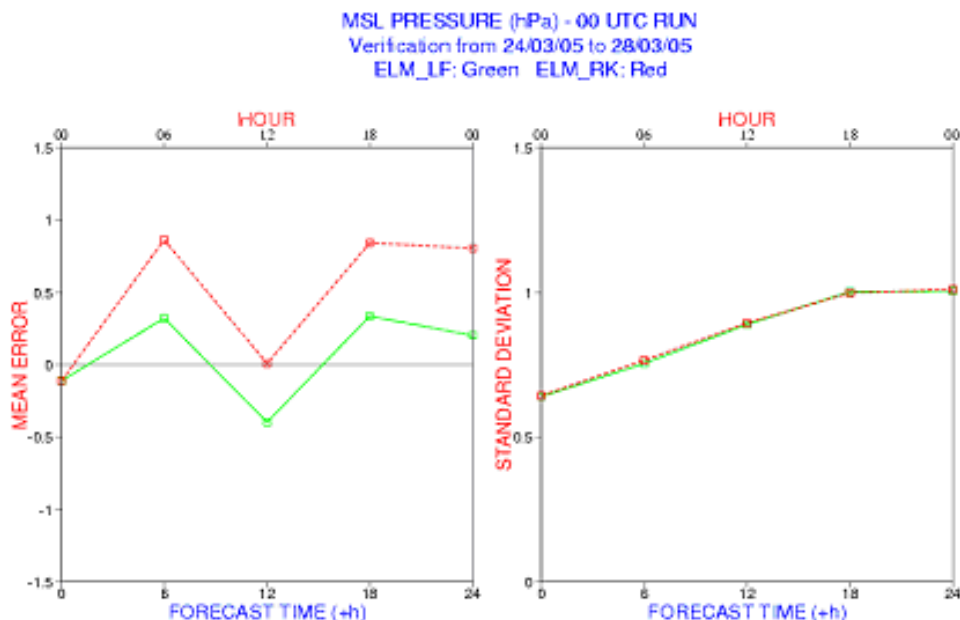
Figure 1: The pressure bias problem in the RK-dynamical core compared to the Leapfrog-scheme.

The pressure bias for RK runs, typically positive, tends to be larger (especially increasing
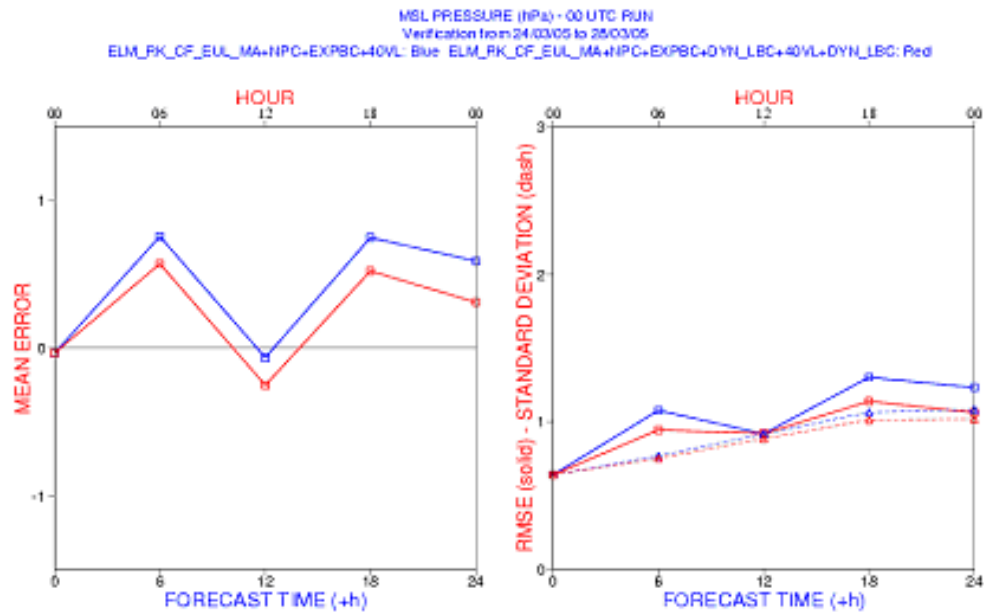
Figure 2: Positive effect of the dynamical bottom boundary condition on the PMSL.

with forecast time) leading to a worse RMSE. The implementation of the Gassmann formulation of the dynamical bottom boundary condition in the vertical pressure gradient term of the horizontal momentum equations brought an improvement in pressure bias behaviour for the RK dynamics (Fig. 2). Other work was done on RK core (change in metric term discretization, change in vertical average on half levels, etc), but no significant positive impact on the pressure bias was found. Objective verification results for the winter period 20 Jan - 04 Feb 2008 showed that 7 km RK/LF differences in pressure bias for COSMO-ME are almost negligible (Fig. 3). Generally, small RK/LF bias differences using 2.8/7 km grid spacing (depending on season, domain, location, etc) are still found (RK larger bias). RK/LF differences in MSLP bias are very big (especially at longer forecast times) using a 14 km grid spacing.

Other experiments showed that the pressure bias problem is not only present by changing the dynamical core (RK/LF), but it is evident also by using very large domain size and particularly clear using a 14 km grid spacing when compared to hydrostatic model runs (HRM). Objective verification results showed a difference in MSLP bias behaviour in 7 km RK (and LF) COSMO runs having domains of different sizes (the larger domain, the greater the bias difference - Fig. 4). Moreover, a large pressure bias difference was also found between 14 km COSMO and HRM runs on a Euro-Atlantic domain (Fig. 5). COSMO LF/RK runs have a larger bias increasing with forecast time. The pressure bias is a characteristics of COSMO model and is probably related to the model formulation. For this reason the effects on the pressure bias of two changes in the model formulation were addressed:

- Gassmann and Herzog (2006) reconsidered the derivation of prognostic temperature and pressure equations to remove some inconsistencies in the formulation of these equations;

- Zängl proposed a new reference atmosphere to overcome the problem of limitation in vertical extent of the model domain using the default reference atmosphere (model implementation in COSMO 4.5, September 2008).
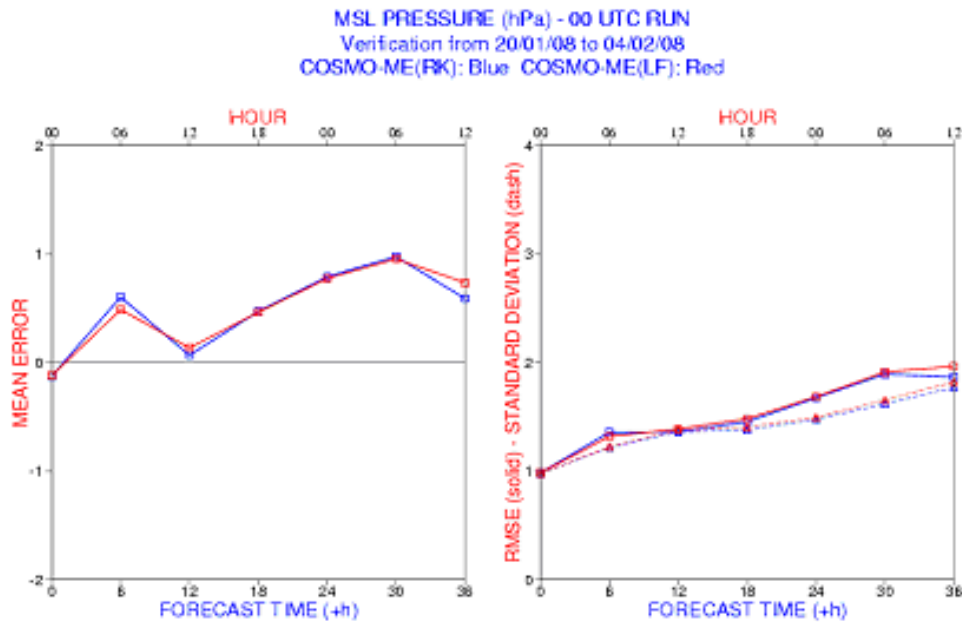
Figure 3: Comparison between RK and Leapfrog, 7 km resolution.

2.1.1   Heat source term in p equation

The pressure bias problem was also found in experiments using a coarser resolution (14 km) and enlarging the domain size (7 km). This could be an indication of some inconsistencies in the formulation of COSMO T/p budget equations. As suggested by Gassmann and Herzog (2006), a possible source of pressure bias could be neglecting the diabatic term in pressure equation. Preliminary real case experiments (winter period) without this approximation showed that the impact on the pressure bias is not general in 7 km runs (a slight deterioration around 12 UTC. Fig. 6), but it is apparent in 14 km runs (Fig. 7). Objective verification results (7 km) for a summer period were not so promising as those for the winter period (Fig. 8). No reduction of the amplitude of the pressure bias variation was found, but only a temporal shift in MSLP bias behaviour was present. More work would be needed. The pressure bias problem is typical for the COSMO model (not only of RK core !) and it seems to be mainly related to the model equation formulation. The use of a prognostic p-equation does not guarantee an exact mass conservation (accuracy depending on numerical algorithm), which is equivalent to introduce artificial sources or sinks in the continuity equation. Problems arise in applications such as data assimilation systems, where the pressure accuracy is important. A more conservative dynamical core is needed for the COSMO model.

2.1.2   New reference state

Introducing a reference state reduces the computational error in the calculation of pressure gradient terms in the equation of motion for not too large deviations of pressure from reference pressure.
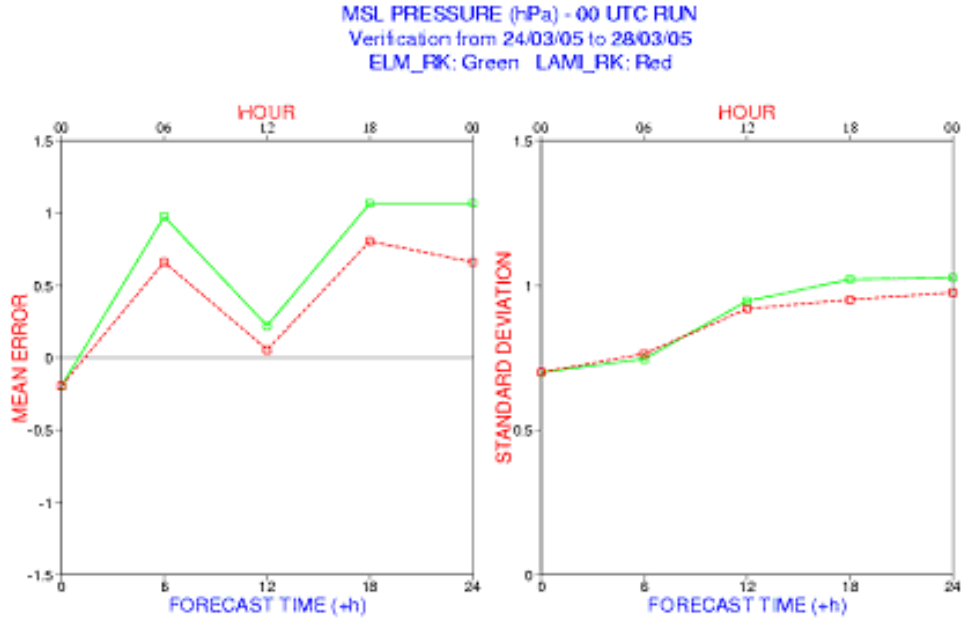
Figure 4: Influence of the domain size to the pressure bias.

At present, the reference atmosphere in the COSMO model is defined through the sea-level pressure, p_{00}, the sea-level temperature, T_{00}, and a generalized vertical temperature gradient

$$\frac{dT_0}{dlnp} = c_1.\tag{1}$$

Integration of the hydrostatic equation yields

$$T_0(z) = [T_{00}^2 - \frac{2gc_1}{R_d}(z - z_0)]^{1/2}\tag{2}$$

and

$$p_0(z) = p_{00}exp(\frac{T_0(z) - T_{00}}{c_1})\tag{3}$$

From that follows

$$\frac{dT_0}{dz} = -\frac{gc_1}{R_dT_0}\tag{4}$$

which implies that the ordinary vertical temperature gradient becomes increasingly negative in the stratosphere. For the default values used in the COSMO model, $p_{00} = 1000$ hPa, $T_{00} = 288.15$ K and $c_1 = 42$ K, the reference temperature reaches 0 K at a height of 28923 m. This is clearly too restrictive for future plans to raise the model top to 10 hPa (about 30 km) or even higher. Another questionable property of the current reference atmosphere is
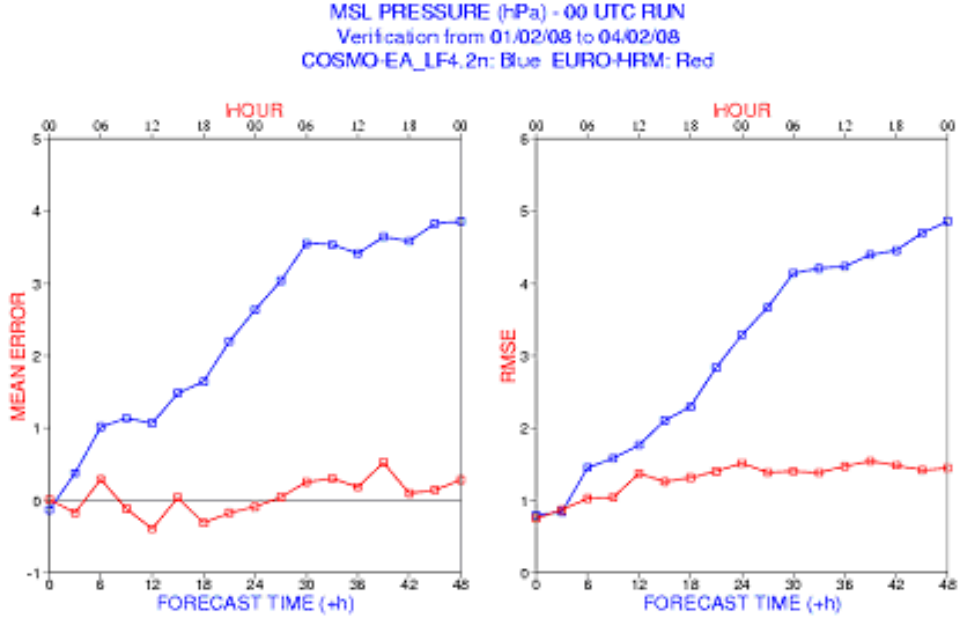
Figure 5: Comparison between COSMO-model and HRM for 14 km resolution.

that the base state pressure does not reach zero where the temperature does so. For the above-mentioned default values, $p_0 = 1.05$ hPa at the height where $T_0 = 0$ K.

To mitigate these problems, a new reference atmosphere has been implemented. Its temperature profile is defined through

$$T_0(z) = T_{00} + \Delta T exp(-z/H) \tag{5}$$

with reference values of $T_{00} = 213.15$ K, $\Delta T = 75$ K, and H = 10 km. For this temperature profile, the hydrostatic equation can be analytically integrated as well, yielding

$$p_0(z) = p_{00}exp[-\frac{gH}{R_dT_{00}}ln(\frac{exp(z/H)T_{00} + \Delta T}{T_{00} + \Delta T})] \tag{6}$$

and

$$T_0(p_0) = T_{00} + \frac{T_{00}\Delta T}{exp(-\frac{R_dT_{00}}{gH}ln\frac{p_0}{p_{00}})(T_{00} + \Delta T) - \Delta T} \tag{7}$$

With this definition, the temperature profile approaches an isothermal gradient in the stratosphere, which

- is closer to reality than an increasingly negative gradient and

- does not impose any limitation on the vertical extent of the model domain.
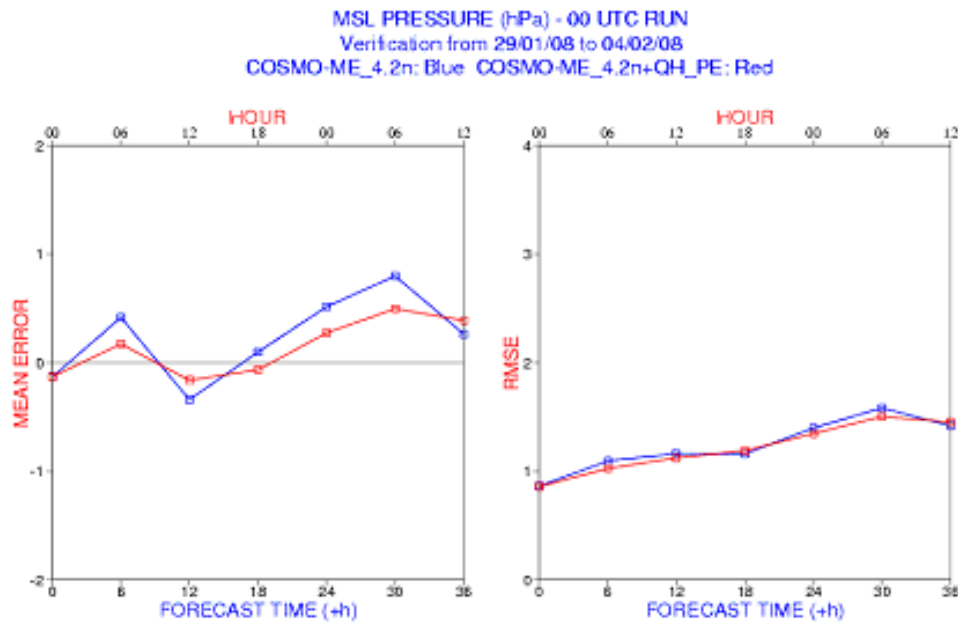
Figure 6: Influence of the diabatic terms in the pressure equations for 7 km resolution.

In the context of implementing the new reference atmosphere, an inconsistency in the computation of the reference pressure at the full model levels has been removed. Up to now, the reference pressure at full levels was set to the arithmetic mean of the reference pressure at the adjacent half levels, which is not consistent with the fact that the geometric height of the full levels is also assumed to be the arithmetic mean of the adjacent half levels. In the revised implementation, two possibilities for initializing the reference pressure are provided, both starting from an arithmetic averaging of height. One method directly uses the analytically integrated hydrostatic equation, the other one numerically integrates the hydrostatic equation from the bottom towards the model top. First experiments conducted with the new reference atmosphere and the corrected initialization of the reference pressure field indicate that both modifications could have a beneficial impact on the surface pressure forecast. Results are presented here for 72-hour forecasts on the COSMO-EU domain, starting on (i) 03 March 2008 (Fig. 9) and (ii) 30 May 2008 (Fig. 10). In all cases, initial data have been interpolated from the GME assimilation run, whereas lateral boundary conditions have been taken from the operational GME forecast. For reference, an experiment using the operational COSMO-EU setup (in particular the leapfrog core) is included. Moreover, an experiment using a non-approximated prognostic equation for perturbation pressure, as recently implemented by L. Torrisi, is shown. The surface pressure field has been validated against interpolated analyzes from GME assimilation runs every 12 hours.

The results reveal several interesting features:

- All experiments, except for the simulation with the non-approximated pressure equation in the March case, show a mostly negative slope in the pressure bias curves, with the bias turning from positive values at early forecast times into negative ones later on.
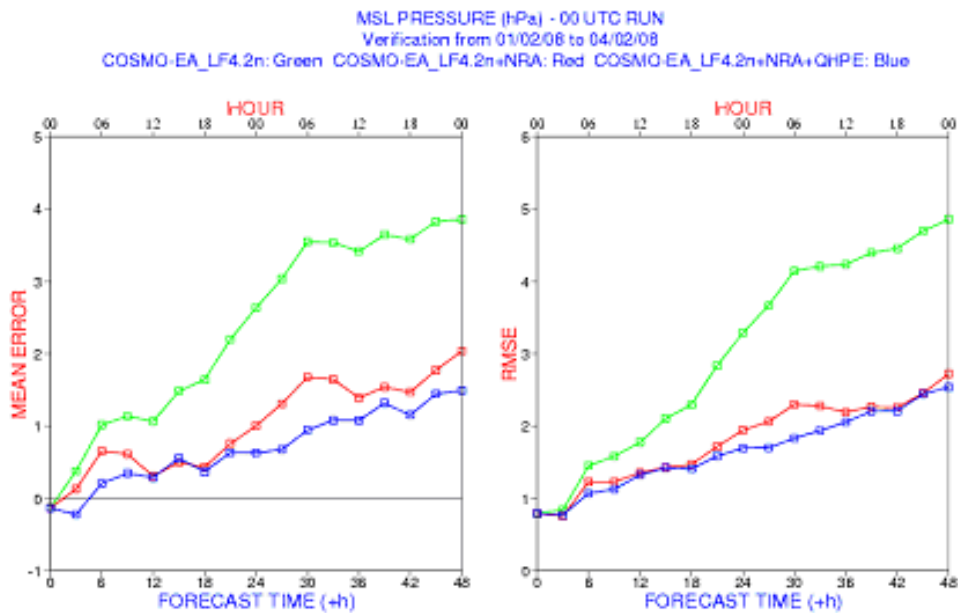
Figure 7: Influence of the diabatic terms in the pressure equations for 14 km resolution.

- Using the analytically integrated hydrostatic equation ("corr 2" in Fig. 9 and Fig. 10) induces a systematically more positive (or less negative) pressure bias than using the numerically integrated equation. This discrepancy is markedly larger for the old reference atmosphere than for the new one, particularly for the March case. Of all experiments using the Runge-Kutta core, the time-averaged bias is smallest when combining the new reference atmosphere with the analytically integrated hydrostatic equation.

- The rms error tends to be somewhat lower with the new reference atmosphere than with the old one. In the cases considered here, the Runge-Kutta core combined with the new reference atmosphere performs similarly well as the old Leapfrog core, whereas somewhat larger rms errors are obtained with the old reference atmosphere.

In summary, the most promising results have been obtained when combining the new reference atmosphere with initializing the reference pressure field from the analytically integrated hydrostatic equation. Thus, longer-term experiments should preferably be carried out with this setting. Objective verification results for only few runs using a 7 km grid spacing for the COSMO-ME showed a slight improvement around 06 UTC (Fig. 11). A dramatic improvement was found for 14 km runs (Fig. 12).
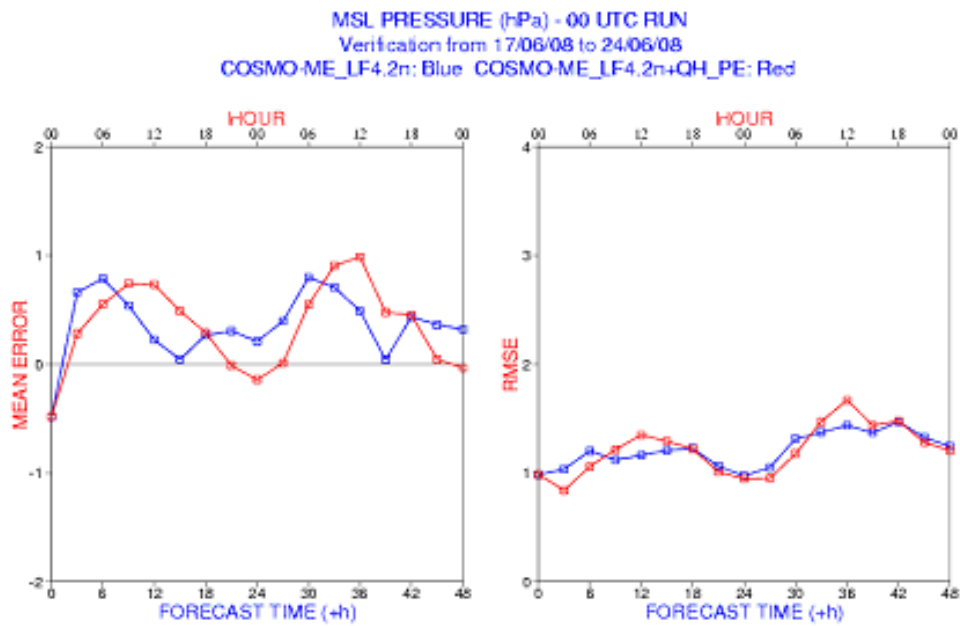
Figure 8: Influence of the diabatic terms in the pressure equations for 7 km resolution; summer period.
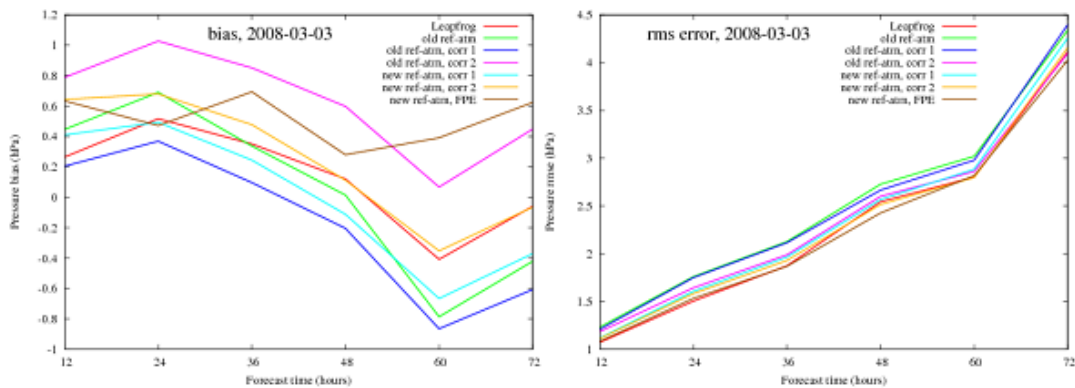
Figure 9: Bias and rms error of the surface pressure field for the experiments started at 00 UTC on 03 March 2008. The experiment denoted as "leapfrog" has been conducted with the operational COSMO-EU setup, all other experiments use the new Runge-Kutta core. The two methods available for calculating the base state pressure are denoted as "corr 1" for the discretized integration of the hydrostatic equation and as "corr 2" for the calculation based on the analytic formula. "FPE" stands for "full pressure equation", using the non-approximated prognostic equation for the perturbation pressure field.
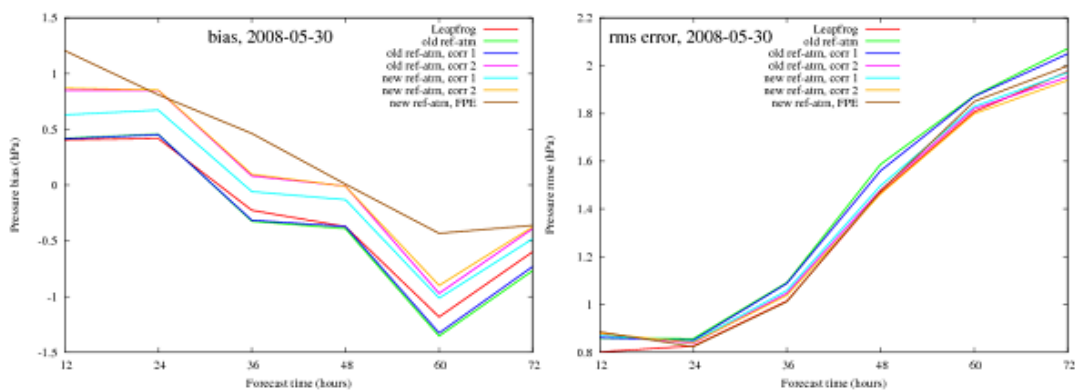
Figure 10: Same as Fig. 9, but for experiments initialized at 00 UTC on 30 May 2008.
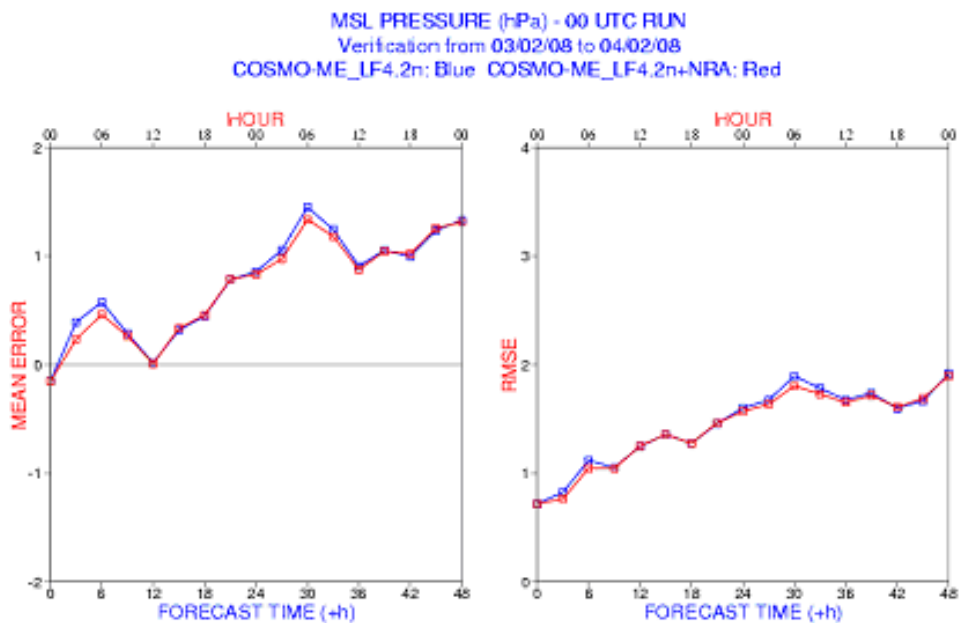
Figure 11: Slightly positive influence of the new reference atmosphere in 7 km runs.
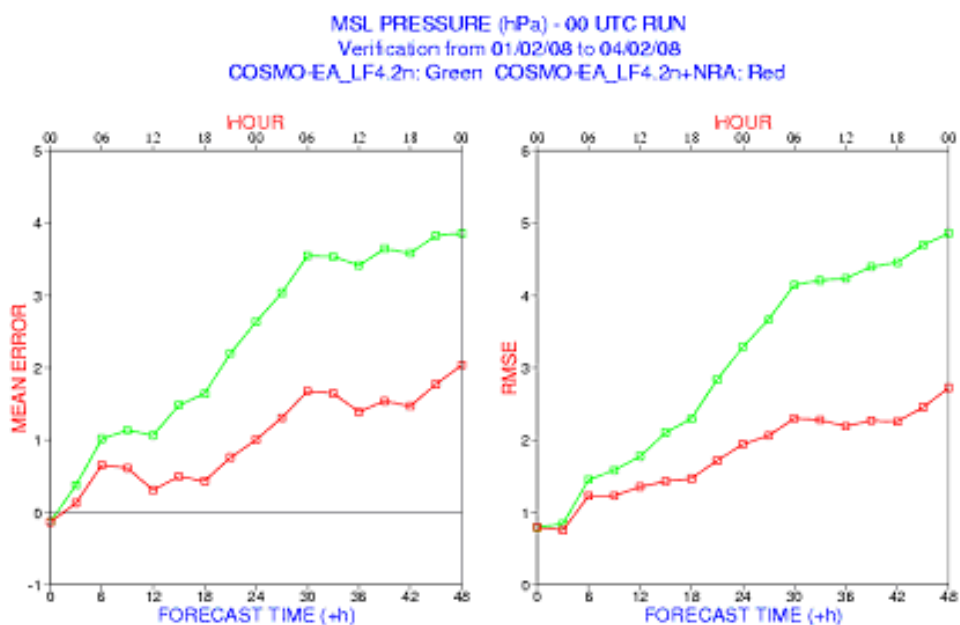
Figure 12: Bigger positive influence of the new reference atmosphere in 14 km runs.

2.2   Task 2: Continue RK case studies

The case studies done at MeteoSwiss were very closely linked with the set-up of the new model cascade which went operational on February 2008. This cascade consists of the new COSMO-7 model which is computed with a grid mesh of 6.6 km (0.06 degree resolution) and the imbedded COSMO-2 model covering the whole Alpine region which has a grid mesh of 2.2 km (0.02 degree resolution). The description of the different configuration of these 2 models can be found under:

$http : //www.cosmo - model.org/content/tasks/operational/default.htm$

One feature is that they are both computed with the same 60 level distribution and use the Runge-Kutta dynamics. Originally it was planned to use a very fine vertical resolution (L60.1) of the planetary boundary layer, i.e. 29 levels below 2 km but operationally the level distribution of the driving model from ECMWF (IFS with 91 levels) was preferred (L60.2). This level distribution uses the bottom 43 levels directly from IFS and adapts the last levels so that the top of the model is at 23.6 km height. The bottom distribution has only 17 levels below 2 km and the level thicknesses are more or less constant (below 500 m) from the height of 5 km up to the tropopause. The problem with the very fine levels was finally solved by the work of Oliver Fuhrer with the stability analysis of the explicit vertical diffusion of TKE (see COSMO General meeting in Kracow, 2008).

2.2.1   First difficulties and their solutions

From a week's visit of Jochen Förstner (DWD) and Günther Zängl (at that time from München University) in March 2006 some interesting results were put together by the participants and are available in a separate Word report in German

$ftp : //ftp.cscs.ch/in/put/abc/morsier/Arbeitstreffen\_Zusammenfassung.doc$

Here are the main outputs:

- extra orographic smoothing, development of the lower bottom boundary conditions, and the p',T'-dynamics (see Task 6);

- the explicit lateral boundary condition helped to solve some of the unstable cases MeteoSwiss encountered but others needed extra horizontal diffusion at the lateral boundaries and just below the Rayleigh damping zone;

- use of the driving model orography at the boundaries with a smooth linear transition over 20 grid points to the high resolution orography in the inner domain (llbc_smooth in INT2LM);

- nice semi-idealized simulation of the thermal circulation in the Inn-valley.

During the whole project period many test cases were evaluated. Starting with 10 weather episodes from high precipitation MAP cases in 1999 to convective, storm and stratus cases and then to verification periods for COSMO 2.2 over the months of July to October 1995, 1997 and 1999 (COSMO-2 for WINDBANK). The encountered instabilities led to the following choices for the configuration of both COSMO 2.2 km and 6.6 km:

(see: $ftp : //ftp.cscs.ch/in/put/abc/morsier/200703\_gdm\_RK\_Langen.ppt$)

- the use of the SL advection of humidity variables instead of the Eulerian Bott 2nd order polynomials. These schemes are positive definite but the SL scheme uses multiplicative filling instead of clipping to achieve this property;

- the use of the standard 3rd order in time RK version instead of the more precise Total Variation Diminishing (TVD) variant which is also 3rd order in time but has less smoothing properties;

- the fixing of a bug in LM2LM in the shift of the boundary layer structure of the temperature (and horizontal winds). This helped to get the model started when downwards extrapolation into deep alpine valleys produced warm air bubbles.

2.2.2   General testing and some verification results

The choices made after the above first difficulties are still operational and the following list shows the systematic verification operated before the introduction of the 2 new models in February 2008:

(i) 6.6 km vs. 7 km

For the winter period a very slight improvement of the wind strength could be seen in the SYNOP verification over the whole domain. There were also some differences in the precipitation at the proximity of the boundaries and this also impacted on the cloud cover. But these effects were not significant.

(ii) Storm 18-20 Jan. 2007 (Kyrill)

This storm event was used to check the stability of the different numerical settings. Curiously the main differences were not seen in the wind speed but in the 2m temperature, on the total cloud cover and the precipitation. This is shown in Fig. 13.
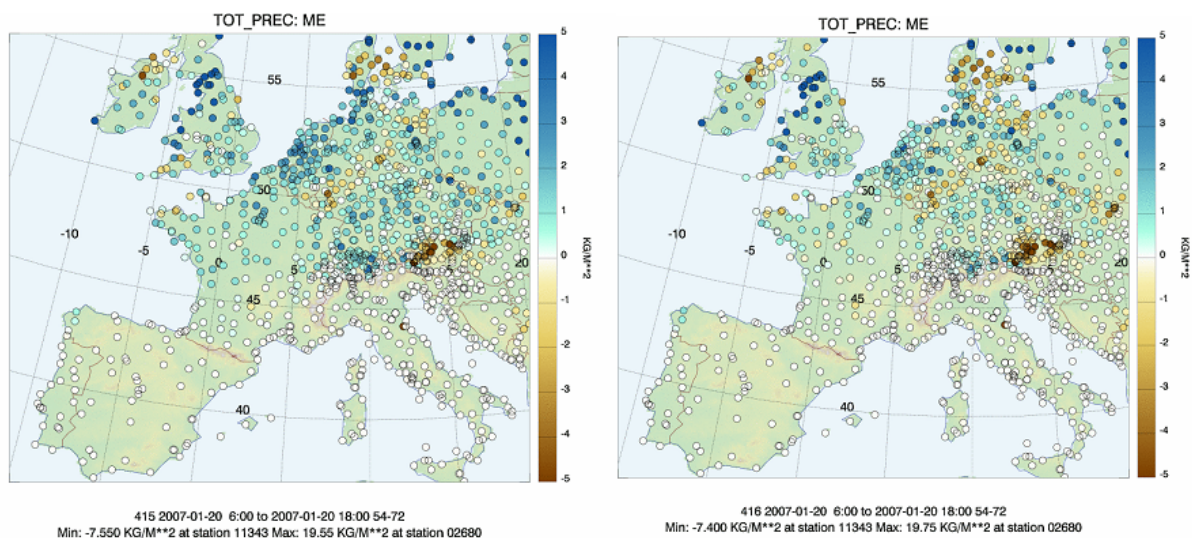
Figure 13: Kyrill precipitation in configuration COSMO 6.6L60.1 (left) and COSMO 6.6L60.2 (right).

(iii) 2.2 km, 7 km, 45 and 60 levels

These experiments were all conducted with their corresponding assimilation cycles to have the best initial and boundary conditions and to prevent differences to come from a common experiment setup. The results are illustrated with the upper-air verification in Fig. 14. There is a problem with the boundary layer of the fine 60 level version (L60.1 of version 424) and these results led to the choice of new vertical levels based on the IFS model (L60.2 of version 427) because the explicit vertical diffusion of the TKE with the very fine vertical model resolution was not stable (see Oliver Fuhrer's presentation at the General Meeting in Kracow in September 2008).

(iv) 2.2 km RK vs. 6.6 km RK vs. 7 km LF

(s3: JuneJulyAugust, s4: SeptOctNov, s1: DecJanFeb)

- S3: The differences in performance are generally small, but in a few cases, there are quite large differences. Notably the standard deviation of the surface pressure error is much decreased in COSMO-2 relatively to COSMO-7. This is probably a direct effect of the better representation of the topography in COSMO-2 and shows the limit of vertically interpolating surface pressure to the station height with a constant gradient. The smaller bias in the 2m-temperature shows that the gradient used in the vertical interpolation to the station high is not optimal. In contrast to surface pressure, using a constant gradient is not a problem, as the standard deviation confirms. Both of these effects show up in the Alpine domain because all stations are used for verification, regardless of the height difference between station and model surface. The precipitation deficit with strong precipitation in COSMO-7 is ameliorated in COSMO-2. The bias and the frequency bias of strong precipitation (> 10 mm/12h) are both much closer to their optimal value 0 and 1, respectively. For 4 different months the following Fig. 15 shows the much better performances of the Runge-Kutta scheme against the operational Leap-Frog for the same horizontal resolution of 7 km;

- S4: The pre-operational COSMO-6.6 with Runge-Kutta integration scheme generally performed about the same or slightly better than the operational COSMO-7 with Leap Frog in October 2007 and Runge-Kutta in November 2007. The exception is cloud coverage, where COSMO-6.6 has a clearly increased positive bias. Large differences are found in the precipitation, which is significantly reduced in COSMO-6.6. The positive bias in COSMO-7 is negative in COSMO-6.6 and slightly larger in absolute value. This is however mainly an effect of the few very much overestimated stations along the model boundary. The positive frequency bias for the smallest threshold (0.1 mm/12h) has decreased. For the largest threshold (10 mm/12h) however, the slight underestimation of the frequency of occurrence in COSMO-7 is amplified to a considerable underestimation in COSMO-6.6. Consequently, the probability of detection drops for this threshold by more than 5%.

(v) 6.6 km vs. 7 km RK

The pre-operational COSMO with 6.6 km resolution generally performs about the same or slightly better than the operational COSMO with 7 km grid spacing. The exception is dew point temperature, where COSMO-6.6 has an increased positive bias, but the standard deviation is still slightly smaller. A special case is the wind speed. It is notoriously underestimated at mountain tops by all COSMO versions due to the non-representativity of mountain tops for grid cell averages. The reduction in wind speed increases this negative bias, but it also decreases the positive bias at many stations in the Swiss Middleland, which is the more important aspect.

The previously found large differences in the precipitation between COSMO-7 and COSMO-6.6 have disappeared due to the fact that both versions now run with the Runge-Kutta integration scheme. Only for the large precipitation (> 10 mm/12h), COSMO-6.6 has a smaller frequency bias.
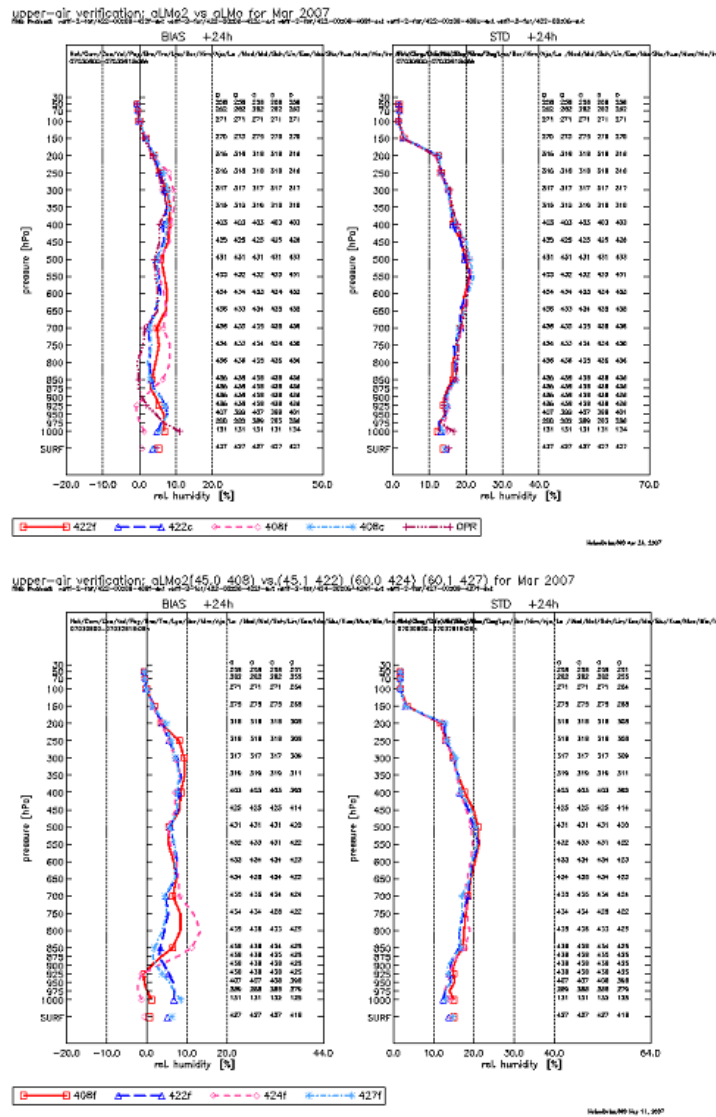
Figure 14: Upper-air (TEMP soundings) relative humidity verification (bias left and standard deviation right) of 24h forecasts in March 2007 for 5 different model versions: OPR: Leap Frog L45; 408: Runge-Kutta 7 km L45, 2 km L60.1; 422: Runge-Kutta L45; 424: Runge-Kutta L60.1; 427: Runge-Kutta L60.2. The letter "c" at the end of the experiment tags stands for coarse (7 km) and "f" for fine (2.2 km).
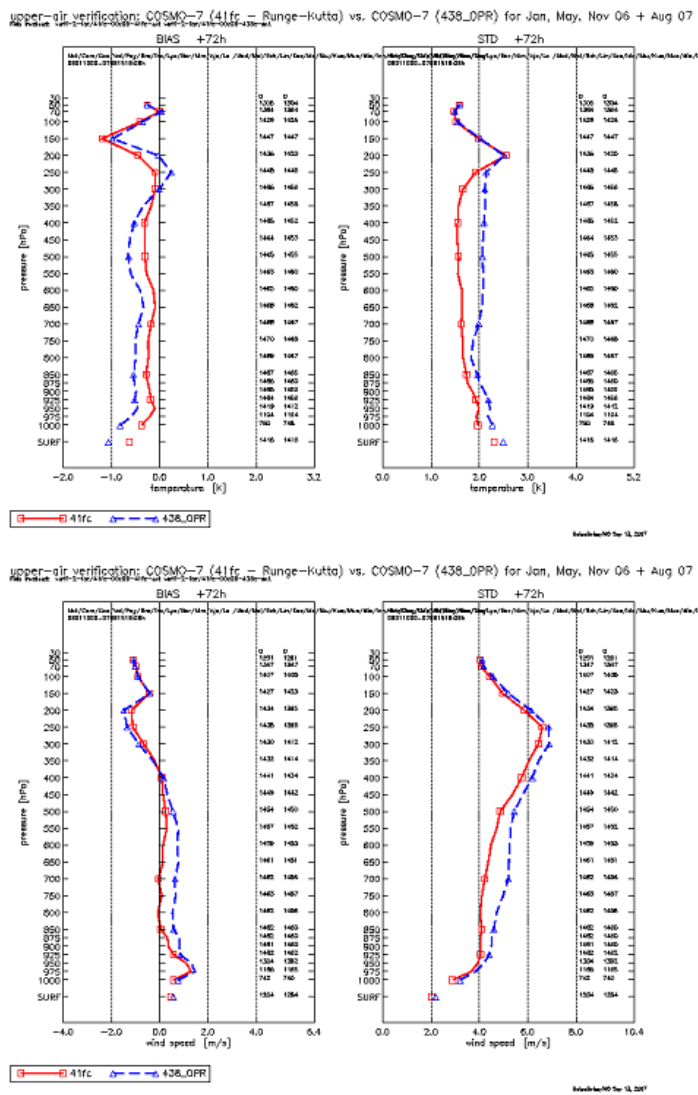
Figure 15: Upper-air (TEMP soundings) temperature (top) and wind speed (bottom) verification of 72h forecasts in Winter, Spring, Autumn 2006 and Summer 2007. The red curves are for the Runge-Kutta version and the blue curves are for Leap Frog.

2.3 Task 3: A Tool for Testing Conservation Properties in the COSMO-Model

2.3.1 Introduction

The fundamental equations of fluid mechanics, especially those used in Meteorology, can be formulated as conservation equations (or at least as balance equations) for mass, momentum and energy, as an example. Therefore a possible conservation of these variables (or others, like potential vorticity) should be obtained in a numerical model. Unfortunately this cannot be achieved in general but is guaranteed at most for a few variables in models which are formulated and also discretized in flux form. In all other cases it would be desirable to determine the strength of conservation violation. To this purpose, a tool was developed to determine budgets of arbitrary scalar variables for the COSMO-Model over an arbitrarily given cuboid volume inside of the model domain (see Fig. 16).
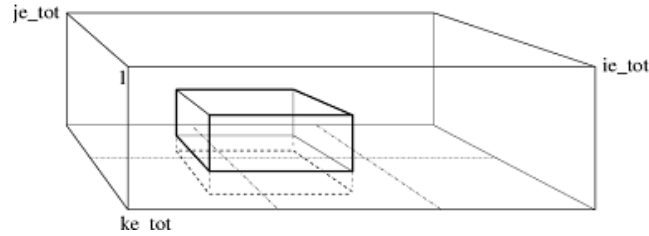
Figure 16: Integration area 'cuboid' lying in the model domain (in the transformed coordinate system). Here, a 3 * 2 domain decomposition is shown.

A general balance equation for a scalar ϕ (a generalized density) with an appropriate flux $\mathbf{f}_\phi$ reads in integral form (i.e. over a steady volume V):

$$\frac{d\Phi}{dt} + F_\Phi = Q_\Phi \tag{8}$$

total amount:

$$\Phi = \int_V \phi dv \tag{9}$$

total flux:

$$F_\Phi = \int_{\partial V} \mathbf{f}_\phi \cdot d\mathbf{A} \tag{10}$$

all sinks/sources:

$$Q_\Phi = \int_V q_\phi dv \tag{11}$$

In the case of ϕ being an integral conservative variable the right hand side of the first equation vanishes and the residuum $Res = d\Phi/dt + F_\phi$ describes the violation of conservation. Consequently, for the determination of these budgets, one has to be able to calculate volume integrals and surface integrals over fluxes in the model. The user of the 'conservation testing tool' first has to define the points in the model area which define the integration box volume (see Fig. 16). The coordinates of the corners of the cuboid imin_integ, imax_integ, jmin_integ, jmax_integ, kmin_integ, kmax_integ are read from the NAMELIST-parameter group DIACTL. In doing this the user is completely independent of any domain decomposition of the model parallelization. Secondly, one has to deliver a scalar field ϕ at the grid

position of the scalars (i, j, k) to calculate the volume integral over it. Thirdly, one has to deliver the vector field $\mathbf{f}_\phi$ whose components are defined at the grid positions of u, v, and w respectively to calculate the flux integral over the surface of the box. The details of the numerical implementation of these integrals and the subroutine calls to use the tool are described in Baldauf (2008b), section 2 and 5, respectively.

2.3.2 'Shift-test'

To test the abilities of the integration tool, a simple 'shift-test' is performed: an initial distribution is given and is simply shifted (or one could say: is transported by a perfect advection scheme) with a constant velocity through the model domain. On a discrete grid there occur some inaccuracies in the balance of this process which will lead to two artifacts. Firstly, a 'volume calculation artefact', which can arise for a transport with a non-integer Courant-number simply by a sampling error (this artefact is partly due to this artificial shift test, it cannot occur in a finite-volume schemes). Secondly, and more important, a 'flux calculation artefact' occurs due to errors in the estimation of the flux field $\mathbf{f}_\phi$ from the neighboring grid point values of ϕ. An unexpected result was that a simple upwind first order calculation is partly better than a second order centered difference or even higher order flux calculation (with or without higher order RK-time integration). However, recent studies by R. Petrik (MPI Hamburg) show that a Lax-Wendroff flux calculation seems to be the best choice. The addition of both artifacts can disturb the balance of conservation. In the tested example a relative error of the residuum of about 10^{-4} occurs. Nevertheless, the simple shift test did not show a significant programming error in the tool.

2.3.3 Weisman-Klemp test case

A first application of the integration tool was carried out with the idealized warm bubble test case (Weisman and Klemp, 1982). An ellipsoidal warm bubble serves as an initial disturbance with an increase of temperature of max $\Delta T = 2$ K. The atmosphere is in steady state at the beginning. The physics parameterizations are completely switched off, only the saturation adjustment (condensation and evaporation) is active. Therefore only water vapor q_v and cloud water q_c can occur. Further on there occur only advective fluxes $\mathbf{v}\rho_x$, but no turbulent or sedimentation fluxes. In Fig. 17 the balance of the moisture mass is shown. During the rising of the bubble (approximately the first 400 timesteps) moist air is sucked especially from the lower portions of the atmosphere. When the buoyancy is reduced, the bubble expands sidewards and blows out the moist air (timesteps 400-600). During this process the positive tendency of the mass change is not very well balanced by the negative tendency of the flux divergence (and vice versa); the residuum is rather big (Fig. 18). And therefore the relative error is about 0.7%. Therefore the question arises if this is a real error in the model or an artefact by the integration tool. Because the (conserving) Bott-advection scheme delivers very similar results, the problem seems not to be due to the Semi-Lagrange advection scheme, which was used here. The error in the total mass calculation of about 0.04% seems to be too small to explain this moisture mass change, too. Further effects of the 'flux integral artefact' could be excluded by an increase of the box volume by a factor of 2 in both x- and y-direction which does not change the residuum. This indicates, that the violation of the conservation is not induced by the inflow through the boundaries, but there seems to be a violation of conservation by the description of the physical process by the model.

A further experiment, where the the saturation adjustment was switched off showed a dras-
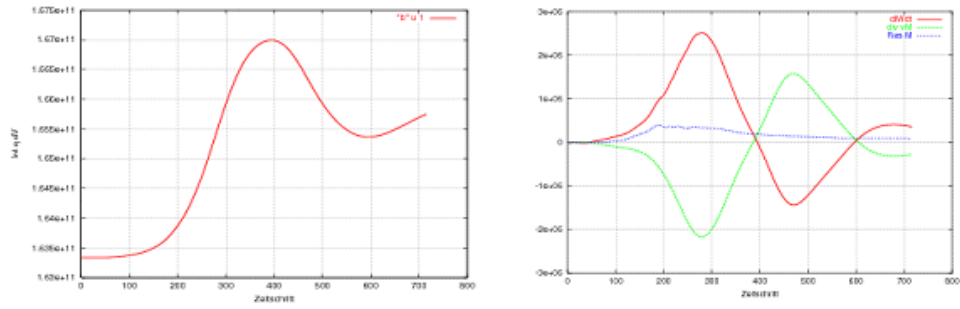
Figure 17: Weisman-Klemp-test case, density of moisture $\rho_x = \rho_v + \rho_c$, total mass of moisture (left); right: balance terms $\Delta\Phi/\Delta t$ (red), F_ϕ (green) and the residuum (blue).
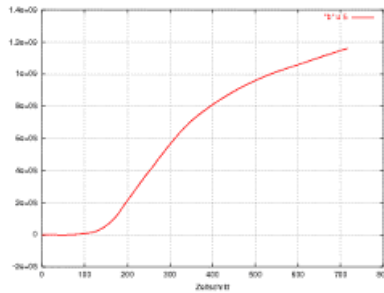
Figure 18: as Fig. 17 for the temporal integral of the residuum ΔM.

tically reduced residuum. This indicates, that the cause for the violation of conservation of moisture mass stems from the saturation adjustment. Indeed, the saturation adjustment in the COSMO-model conserves the specific mass (and specific energy) but not mass (and energy) themselves. This test serves as a first example to show in which way such a conservation testing tool can find hidden inconsistencies of the model. Although such a tool itself has some inherent, sometimes misleading properties as was discussed shortly for the 'shift-test', it can be used successfully at least in idealized simulations and can give valuable hints for the violation of conservation properties.

2.4   Task 4: Advection of moisture quantities in conservation form

This task is described in more detail and with further references in Förstner, Baldauf, and Seifert (2006). In the beginning of the development of COSMO-DE stable integration of the prognostic equations for the moisture quantities (q_x) was realized by doing two sequential Eulerian advection steps with half the time step of the dynamics to ensure Courant numbers less than one. Furthermore, to deal with the transport equations in advection form, after calculating the flux divergence the additional divergence term was subtracted, thereby destroying again the positive definiteness of the flux form advection scheme ("Flux Form - DIV"). Skamarock (2006) summarizes and presents ideas which combine several desirable properties of transport schemes used up to day. He concentrates on Eulerian schemes in flux-form and addresses splitting errors, mass conservation, Courant number restriction and positive definiteness. Following these ideas different schemes were implemented in the COSMO-DE in a Courant number independent (CRI) way. To switch to a "Conservation Form" of the equations, the specific moisture quantities are first multiplied with the air density. Then the resulting densities are transported and finally transformed back into the specific values. To do this a value for the air density, which was updated using the same advection scheme as for the moisture, is used. Since the advection is split into separate 1D steps for the different directions, a Strang-splitting approach is used to reduce the splitting error. To circumvent the Courant number restriction, the Courant number at each cell face is broken up into an integer and a remaining fractional part. While flux calculation is quite simple for the integer part only, the fractional part is dealt with a more sophisticated flux form transport scheme which is normally restricted to Courant numbers less than one. As a scheme with rather low numerical diffusion, a CRI version of Bott's (1989) positive definite advection was implemented into the COSMO-DE. The Bott scheme is realized in two variants with either second or fourth order polynomials for the calculation of the integrated (fractional) fluxes. When we compare the CPU time for a real case simulation, where advection is calculated for all six prognostic moisture variables q_v; q_c; q_i; q_r; q_s and q_g, while the fourth order version is slightly more expensive, the second order one is comparable to the semi-Lagrangian transport in this respect. All in all with the CRI version of the Bott scheme we get a high-order positive definite scheme at a reasonable computational cost. To verify the correct implementation and for comparison of the different schemes idealized advection tests were carried out with the COSMO-DE. As a first and also very common test, the solid body rotation of a tracer cone was simulated (Fig. 19). In the case shown, the angular velocity was rather high, leading to Courant numbers well above one. The schemes perform equally well, at least in two aspects: first the Courant number independence is fulfilled, since in each case we get a stable integration; second the circular shape of the cone is more or less retained, i.e. errors due to the directional splitting method used for the Bott scheme are negligible.

A tracer experiment where an almost uniform tracer distribution was transported in the flow field of a real case study clearly showed that it is not a good idea to use the "Flux Form - DIV" variant mentioned above and the "Conservation Form" of the equations is clearly to be preferred. Further details can be found in the newsletter article. The 2nd order Bott scheme is currently used for the advection of the moisture variables in the COSMO-DE. Additionally the Bott advection was tested in the COSMO-EU in a quasi operational setup. These tests were run over periods of several months. While most of the time these runs performed well and without serious deficiencies, a crash of the model could be traced back to the moisture advection. In this case the splitting error due to the splitting of the horizontal and vertical directions in combination with a very steep slope of the terrain led to this failure. Similar results were obtained at MeteoSwiss where the scheme failed in several cases due to the steep slopes in the Alpine region. It is possible to reduce the splitting error by a more complete
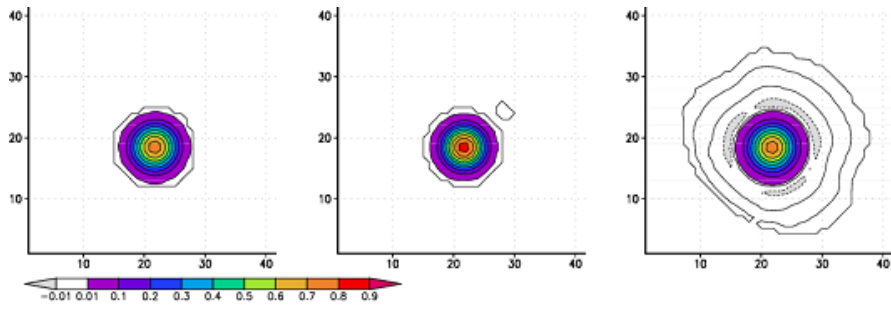
Figure 19: Solid body rotation of a tracer cone with an initial maximum of 1.0. Results after 80 time steps equivalent to one revolution. The Courant Number in the domain is close to a value of 3 near the lateral boundaries and approximately a value of 2.2 at the centre of the cone. Left: Bott (2nd order); Middle: Bott (4th order); Right: semi-Lagrange (tri-cubic).

but also more expensive (by a factor of 5/3 for the advection) form of the Strang splitting. In contrast, the semi-Lagrange advection is a multi-dimensional scheme, which needs no directional splitting and therefore proofed to be more robust in these situations. But it has the disadvantage to be a non-positive definite scheme, for which a simple clipping violates the conservation. This can be cured in a rough manner by a global acting multiplicative filling algorithm. In verifications done at CNMCA, the semi-Lagrangian scheme also gave slightly better scores for 7 km runs.

2.5   Task 5: Investigation of convergence

The aim of Task 5 is to study and analyze convergence properties of the Runge-Kutta dynamical core at high resolutions. Such properties can be inspected by considering different horizontal resolutions and a very good resolved vertical coordinate. Tests where done with:

- 2-dimensional linear mountain flows, both hydrostatic ($Na/U \gg 1$) and non-hydrostatic ($Na/U \sim 1$),

- 2-dimensional non-linear mountain flows ($NH/U \sim 1$),

- 3-dimensional mountain flows

For all mountain sizes 4 or 5 different horizontal resolutions were tested, in order to evaluate the spatial convergence of the scheme. For all cases the Brunt-Väisälä frequency N has been set equal to 0.01 Hz and the basic flow velocity U is 10 m/s. The mountain ridge has a Gaussian shape, $h(x) = H exp[(-x^2/a^2)log2]$, where H is the mountain maximum height and a (the mountain width) is the horizontal distance from the mountain top where the height is H/2. The following results are all performed with the p'T'-dynamics. The Rayleigh damping layer starts at 11 km.

Several error measures (error norms) for the variables vertical velocity, kinetic energy, wave drag, U-momentum component were inspected:

- $L0 = \max \mid F - F_{finestmesh} \mid$

- $L1 = 1/N \sum \mid F - F_{finestmesh} \mid$

- $L2 = [1/N \sum (F - F_{finestmesh})^2]^{1/2}$

The reference solution in each case is a high resolution simulation on the finest mesh. The summation is performed over a subdomain containing the mountain.

The mountain wave drag will be computed by integrating the surface pressure in the x-direction.

$$D = \sum p'(x,0)dh/dx\Delta x \tag{12}$$

The vertical flow of the U- momentum component will be computed at each grid level by summing up all the cells in a grid level

$$D(z) = - \sum \rho_0(z)u'(x,z)w'(x,z)\Delta x \tag{13}$$

The values obtained will be compared, if possible, with the analytical solution (available in the linear hydrostatic case). To extract the effect of the improved horizontal discretization schemes, a very good resolved vertical coordinate $\Delta z = 100$ m was used which at least for the hydrostatic test cases should always lead to well converged solutions. There occurred some problems with the inflow and outflow boundaries, where the vertical velocity had positive values partially in the same order as the signal from the mountain (see Fig. 20, left). This error is too small to be noticeable in real-case applications; however, it becomes evident in idealized simulations with constant flow and a very low mountain (or no mountain at all). These artifacts could be reduced by initializing with the reference state, i.e. to set p'=0 and T'=0. An alternative solution for this problem was found by G. Zängl: the perturbations occur because the present initialization of the perturbation pressure field (executed in

src_artifdata for idealized simulations, otherwise in int2LM) is not exactly consistent with the discretized buoyancy term in the vertical momentum equation. To fix the problem, a new initialization procedure has been developed by solving the discretized vertical wind equation (for dw/dt = 0) for p'; ideally, this would ensure strict absence of buoyancy at the lateral model boundaries. The improvement by this measure can be seen in Fig. 20 (right).
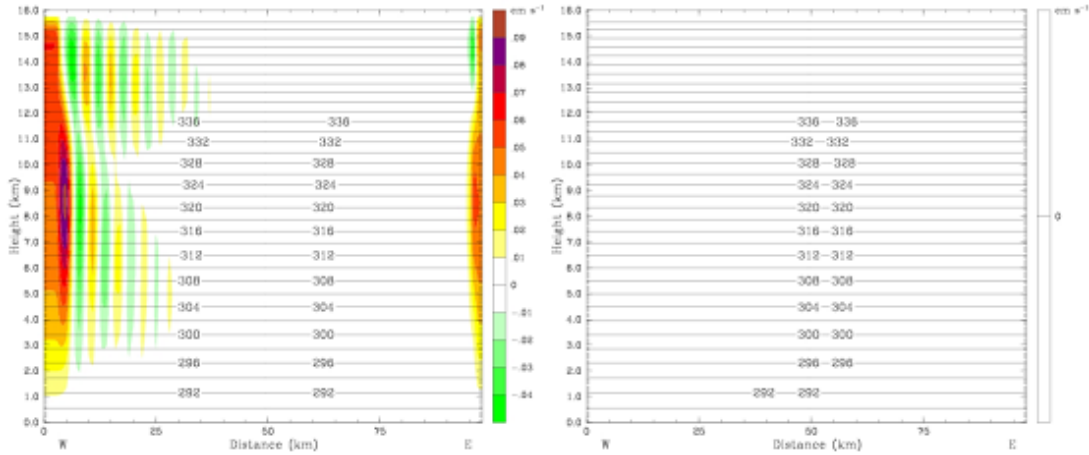
Figure 20: Comparison of the old p' initialization (left) which delivers error amplitudes of about w ∼ 1 mm/s and the new one (right) with error amplitudes of w ∼ 10^{-4} mm/s. Simulation with flat surface, u = 10m/s, and fixed relaxation b.c.'s, t = 12 h. Fields: Θ (contour interval 2 K), w (colors).

2.5.1   Hydrostatic linear mountain flow simulations

In case of a hydrostatic 2-dimensional mountain flow (mountain width a=10 km, mountain height H=10 m and U/Na=0.1), simulations have been performed with constant horizontal resolution Δx equal to 4000 m, 2000 m, 1000 m and 500 m, along either x- and y- directions ($\Delta x = \Delta y$). The extension in y-direction always covers 7 cells. The mountain ridge is located in the middle of the domain. As mentioned Δz=100 m with 195 vertical levels was set. The total simulation time is 60 h. For all the resolutions the same timestep dt=2.5 sec was used with a domain size of 500x19.5 km^2. The chosen horizontal resolutions are 4 km, 2 km, 1 km, 500 m (250 m). A comparison of L0, L1, L2 error norms for vertical velocity and kinetic energy for the two versions of the 3rd stage Runge-Kutta (TVD and 'standard') is shown in Fig. 21. The differences between the two schemes are quite small (note that for the TVD scheme the plot shows also the 250 m resolution), and only a small advantage of the 'standard' RK3 (Wicker and Skamarock, 2002) compared to the TVD-RK3 can be detected. The convergence is less than 2nd order for the resolutions simulated here, but the plots for the kinetic energy show that a nearly 2nd order convergence is approached for higher resolutions.
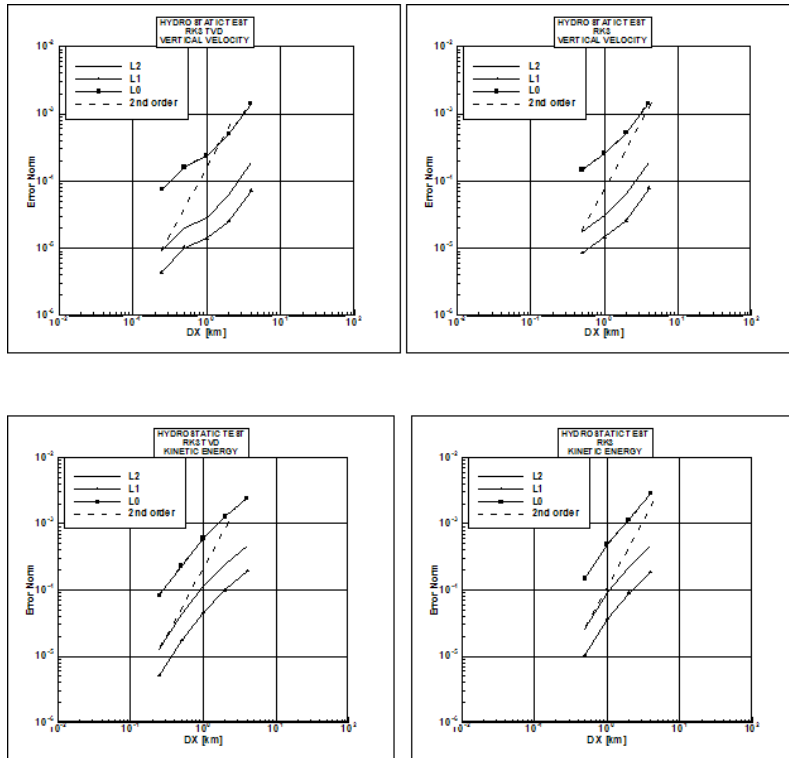
Figure 21: error norms L0, L1, L2 for vertical velocity and kinetic energy for the TVD Runge-Kutta and the standard Runge-Kutta scheme in the hydrostatic linear case. Dashed lines indicate 2nd order convergence.

2.5.2   Hydrostatic non-linear mountain flow simulations

Now the mountain has a height of H = 500 m with the same width than before (a=10 km). The simulation time had to be chosen a little bit longer to attain stationary results (Time = 100 h). Again the same time step dt = 2.5 sec has been chosen. The domain size was 500x19.5 km^2 and the horizontal resolution is 4 km, 2 km, 1 km, 500 m, (250 m). The height of the mountain was chosen in a manner that any non-stationary effect should occur. As the theory foresees, the wave breaking over a gaussian ridge takes place for NH/U>0.85 (which means H>850 m). Whereas the kinetic energy behaves completely similar for the two RK-schemes, the vertical velocity converges better in the TVD-variant.
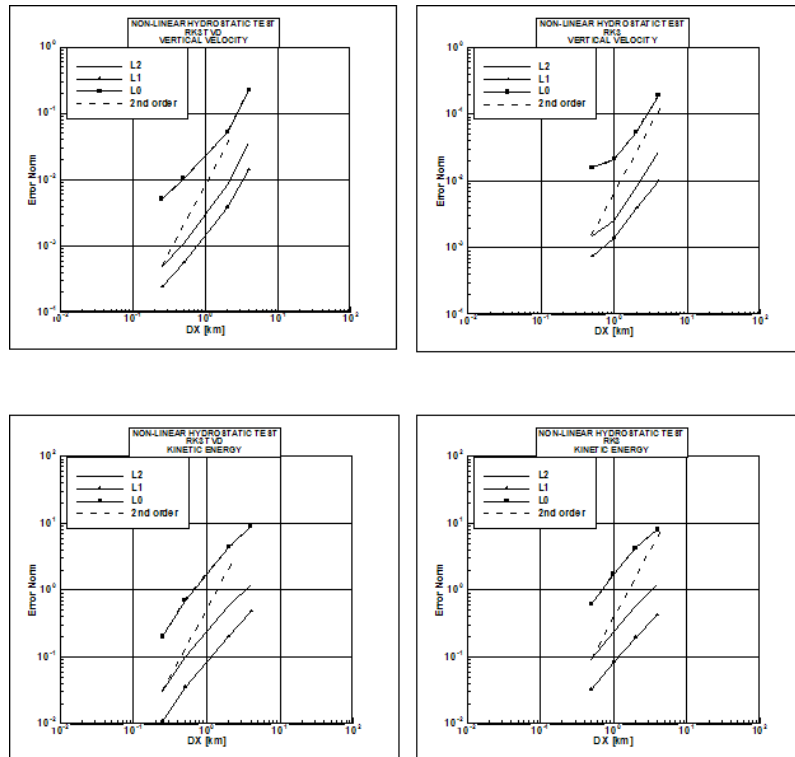
Figure 22: error norms L0, L1, L2 for vertical velocity and kinetic energy for the TVD Runge-Kutta and the standard Runge-Kutta scheme in the hydrostatic non-linear case. Dashed lines indicate 2nd order convergence.

2.5.3   Non-hydrostatic linear mountain flow simulations

In case of non-hydrostatic mountain flow (mountain width a=500 m, mountain height H=10 m which leads to U/Na=2.0), simulations with a constant horizontal resolution equal to 2000 m, 1000 m, 500 m, 250 m and 125 m ($\Delta x = \Delta y$) have been performed. Also in this case Δz has been set to 100 m and 195 vertical levels have been used. The total simulation time is 100 h, dt = 2.5 sec, and the domain size is 250x19.5 km^2; the horizontal resolutions are 1 km, 500 m, 250 m, 125 m. In this case no differences can be seen for the two RK-variants (Fig. 23 and Fig. 24).
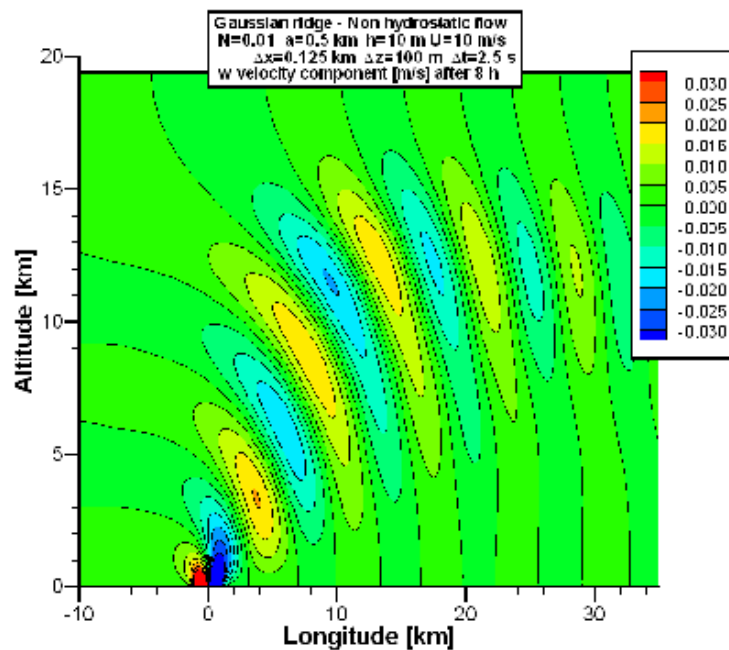
Figure 23: Non-hydrostatic flow example: vertical velocity.
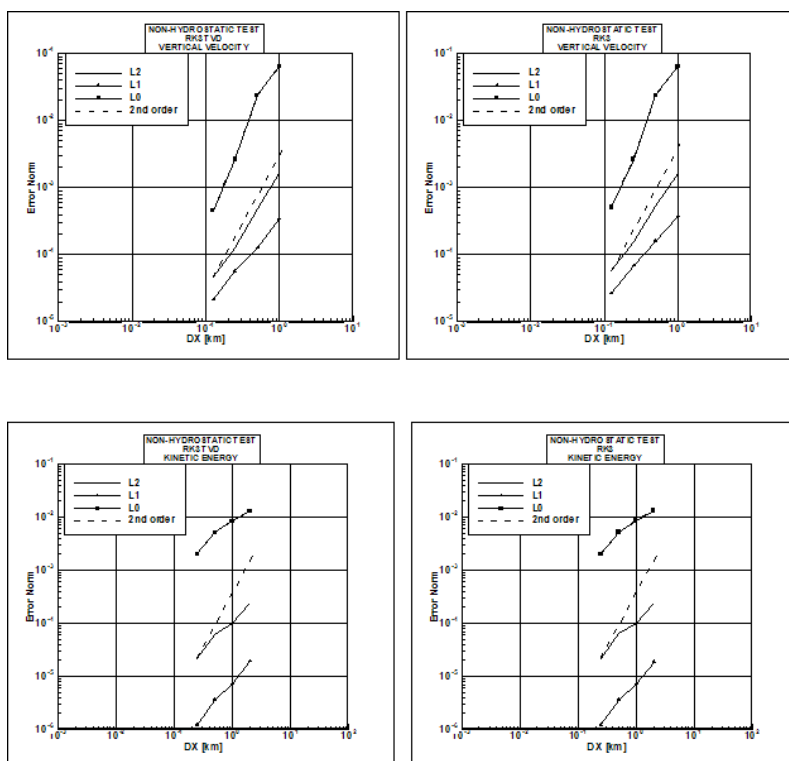
Figure 24: error norms L0, L1, L2 for vertical velocity and kinetic energy for the TVD Runge-Kutta and the standard Runge-Kutta scheme in the non-hydrostatic linear case. Dashed lines indicate 2nd order convergence.

2.5.4   3D mountain flow tests

In Gassmann (2002), chapter 5, the flow solutions obtained with different time integration schemes (Leap Frog and Runge Kutta) and resolutions for an Agnesi mountain were simulated and showed a rather different behaviour for different resolutions. The idea is to show that a similar behavior is only due to the different spatial scheme (i.e. 3rd order and 5th order upwind), and to the grid size.

In the present test case the mountain has again a gaussian shape, h=750 m, and a=10 km. It was not possible to get a steady solution for a 1500 m high mountain as in Gassmann (2002). The grid spacing ranges from 16 km to 4 km (smaller sizes up to 0.5 km were tested, but the solution does not change significantly) and the horizontal domains are 352 km x 352 km for the 16 km grid, 256 km x 256 km for the 8 km grid, 256 km x 128 km for the 4 km and smaller meshes (not shown here). Again 195 vertical levels with constant spacing of 100 m have been used. Reference dry atmosphere has been defined with constant Brunt-Väisälä frequency N=0.01 s^{-1}, ground Temperature 15 Celsius and ground pressure 10^5 Pa. Basic flow velocity U=10 m/s. Test runs were carried out for 20 hours, that is enough for disturbances traveling at 10 m/s to be advected away from the flow domain.

All the test cases have been computed with 3rd order Runge Kutta TVD time integration scheme (RK3), setting the iadv_order input parameter to 5 (that is indicated as UP5 in the pictures) and 3 (UP3 in the pictures).

In Fig. 25 something similar to Gassmann (2002), fig. 5.1 is shown, i.e. the vertical velocity component for different resolutions at the symmetry plane of the flow domain. The pictures cut away most of the Rayleigh damping layer, that starts from an altitude of 11 km and is 85 levels thick. In Fig. 26 the horizontal velocity component at the ground level is shown. The differences between the UP5 and UP3 schemes are visible. Note that in the coarsest resolution among the tests in Gassmann (2002) the grid size was about 3 times the mountain width (7 km / 2.6 km), that might explain the larger differences there.

The following conclusions from the convergence tests can be drawn:

- for 2D flows:

    - slightly less than 2nd order spatial convergence was reached. Obviously the convergence rate is dominated by the 'weakest' discretization, the fast waves scheme;

    - TVD and non-TVD 3 stages Runge Kutta show similar behaviour with slight advantages of the standard scheme in linear cases and slight advantages of TVD in non-linear cases;

    - the time step has minor effect (if any) on spatial convergence;

    - 2D flow tests are rather sensitive to a proper parameter setting for the upper and lateral boundary conditions (damping layers); fortunately these sensitivities are much less for 3D flows;

    - it was difficult to compare with analytical solutions (Baldauf, 2008c), due to boundary conditions (see below).

- for 3D flows:

    - the optimal damping parameter dt*nrdtau increases to $\sim$ 1000 s;

    - with poor resolutions different schemes can give different solutions. This is an indication that the resolutions are far from convergence. Here the higher order upwind schemes can improve the results (see Fig. 25 and Fig. 26);

– during this task, a program to calculate linear solutions for flow over mountains with very few approximations was developed. The theory behind it and implementation details are described in Baldauf (2008c). Fig. 27 shows the quite good similarity between this linear analytic solution and the COSMO-model simulation over a bell-shaped mountain with a high frequency modulation.
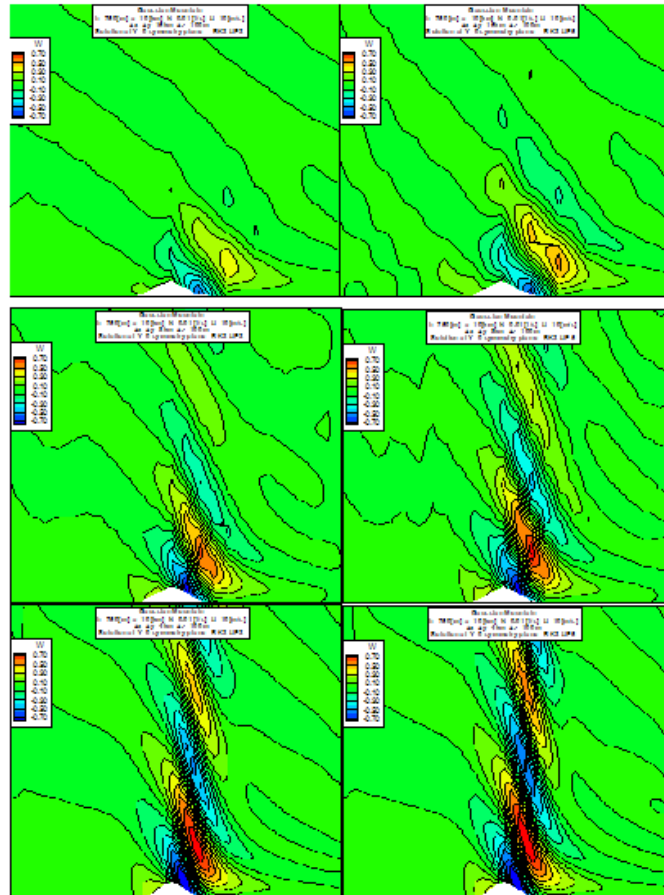
Figure 25: Velocity vertical component at the symmetry plane. On the left: solutions obtained with 3rd order upwind. On the right: solutions with 5th order upwind. From top to bottom horizontal grid spacing: 16 km, 8 km, 4 km. The horizontal size of the picture ranges from -96 km to 96 km, the vertical size from 0 to about 12.65 km.
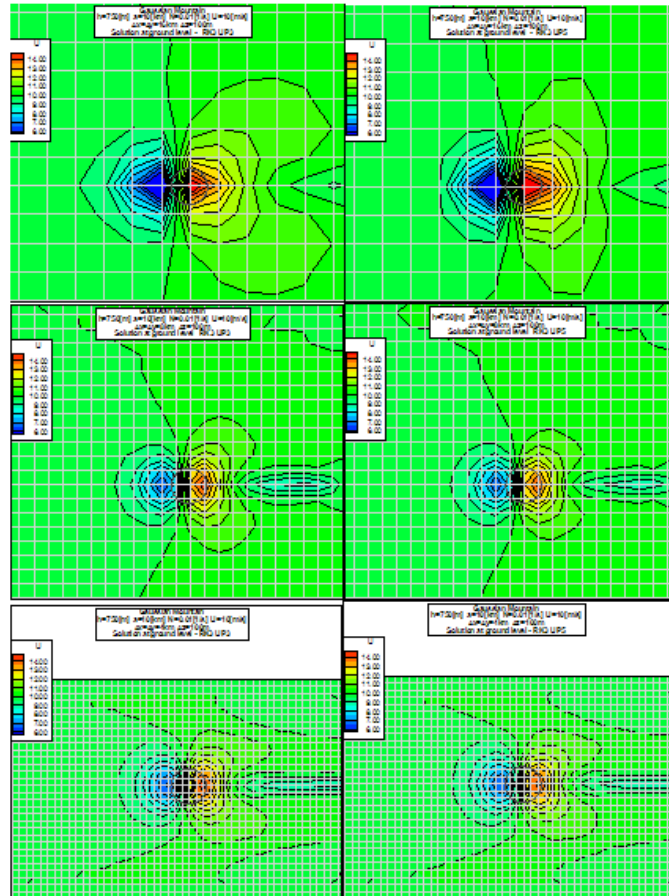
Figure 26: Velocity longitudinal component at the ground plane. On the left: solutions obtained with 3rd order upwind. On the right: solutions with 5th order upwind. From top to bottom horizontal grid spacing: 16 km, 8 km, 4 km. A gray circle (radius 10 km) indicates the mountain position.
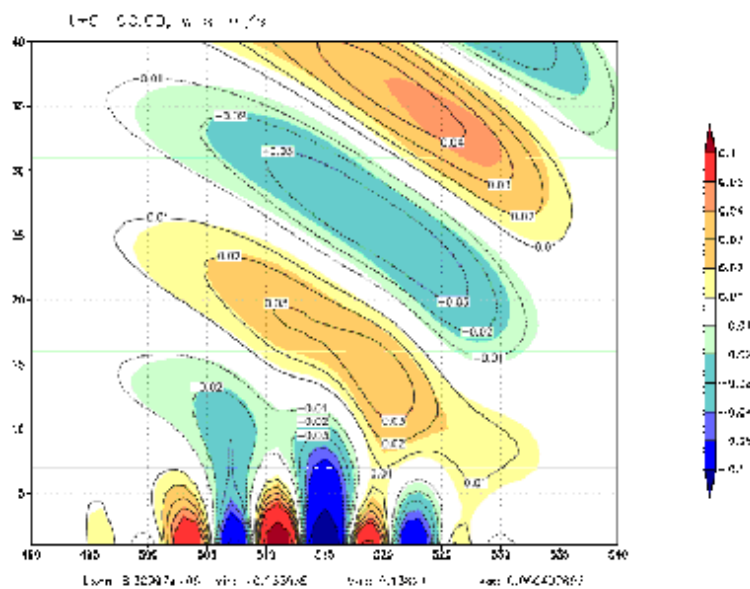
Figure 27: Comparison of the vertical velocity between COSMO-Simulation (colors) and the analytic solution (contours).

2.6   Task 6: Deep valleys + Task 7: Different filter options for orography

Task 7 is closely linked to task 6 since the filtering of orography is one measure to circumvent the problems in deep valleys. Namely the formation of unrealistic cold (or sometimes also hot) spots in the Alpine region. An example is given in Fig. 28 where on the left side a temperature plot of the Alpine region is given. In this case (3 Feb. 2005) the temperature in the first model layer reached an erroneous minimum of $\approx$200 K. The introduction of the "Dynamic Bottom Boundary Condition" (DYN_BBC) (Gassmann, 2004) was the key measure to circumvent the cold pool problem. This can be seen in the temperature difference plot in the right part of Fig. 28. The temperature in the run with the new bottom boundary condition is more than 70 K higher in the problematic region, i. e. no cold pool builds up. It can also be seen, that the changed BBC leads to significant changes only in the orographically structured regions. The basic equations for the DYN_BBC can be found below. For the layer right above the ground, the normal centered-difference approximation of the vertical pressure gradient term in the horizontal momentum equations ($\partial p^*/\partial \zeta$) is deteriorated. In the new formulation the momentum equations are set into the condition given in eq. 17.

$$\frac{\partial u}{\partial t} = -\frac{1}{\rho a cos\varphi}\left(\frac{\partial p^*}{\partial \lambda} + \frac{J_\lambda}{\sqrt{G}}\frac{\partial p^*}{\partial \zeta}\right) + f_u \tag{14}$$

$$\frac{\partial v}{\partial t} = -\frac{1}{\rho a}\left(\frac{\partial p^*}{\partial \varphi} + \frac{J_\varphi}{\sqrt{G}}\frac{\partial p^*}{\partial \zeta}\right) + f_v \tag{15}$$

$$\frac{\partial w}{\partial t} = \frac{1}{\rho\sqrt{G}}\frac{\partial p^*}{\partial \zeta} + g\frac{\rho_0}{\rho}\left(\frac{T-T_0}{T} - \frac{T_0 p^*}{T p_0}\right) + f_w \tag{16}$$

$$\frac{\partial \dot{\zeta}}{\partial t} = \frac{1}{\sqrt{G}}\left(\frac{1}{\rho a cos\varphi}\frac{\partial z}{\partial \lambda}\frac{\partial u}{\partial t} + \frac{1}{a}\frac{\partial z}{\partial \varphi}\frac{\partial v}{\partial t} - \frac{\partial w}{\partial t}\right) = 0 \tag{17}$$

In this way a dynamical expression for the vertical pressure gradient terms is found. The introduction of new filter options for the orography also helped to deal with the problems arising in deep valleys. A set of discrete local (i.e. applicable directly in the physical space) filters of different filter widths is used to filter the orography data. Their local nature makes it easy to combine the treatment with a local condition for the individual grid points. For the COSMO-DE first the orography is filtered globally to remove scales approximately smaller than 4Δ. In a second step a stronger filter (5Δ) is used for all points with a step of the orography still bigger than 625 m.
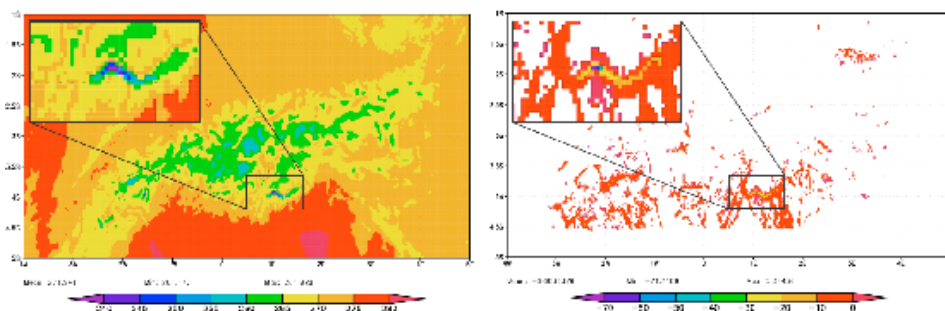
Figure 28: Left: Temperature in the lowest model layer in the Alpine region (init: 00 UTC, date: 2005020317) for a run using the old BBC. Right: Temperature difference of two runs using the old ("NO_DYN_BBC") and the new dynamic ("DYN_BBC") bottom boundary condition, i.e. "NO_DYN_BBC" - "DYN_BBC". Differences smaller 1 K are masked out.

2.7   Task 8: Higher order discretization in the vertical

For a model with increasing resolution, the vertical advection process gets increasing significance. This is the case in particular for convection resolving models with high vertical velocities and therefore a big amount of vertical transport. Due to the fact that the grid levels have a small distance in the lower part of the model, the vertical Courant numbers can reach values bigger than 1. This fact prevents the use of an explicit scheme. Indeed in the WRF model an explicit scheme is used also in the vertical. Tests with COSMO-DE (2.8 km horizontal resolution) show that a significant fraction of grid points in the model domain have vertical Courant numbers bigger than 1. To use an explicit scheme some sort of friction or simply a limitation of vertical velocities is needed. But this measure seems not adequate in a model which should not damp the resolved convection. The current model version contains an implicit scheme using centered differences 2nd order. It is absolutely stable but is not very accurate. Therefore an implicit scheme of 3rd order was implemented. It shows a better behaviour than the 2nd order scheme as can be seen in Fig. 29. But using this scheme in every Runge-Kutta step (as it is done with the 2nd order scheme) causes an increase in the overall computation time of about 30% and therefore is not ready for operational use. This amount can be hardly reduced by optimizing the scheme itself because each of the two steps, calculation of the coefficients of the 5 band diagonal equation system, and solving the linear equation system with a direct 5 band diagonal solver, takes approximately the same time.
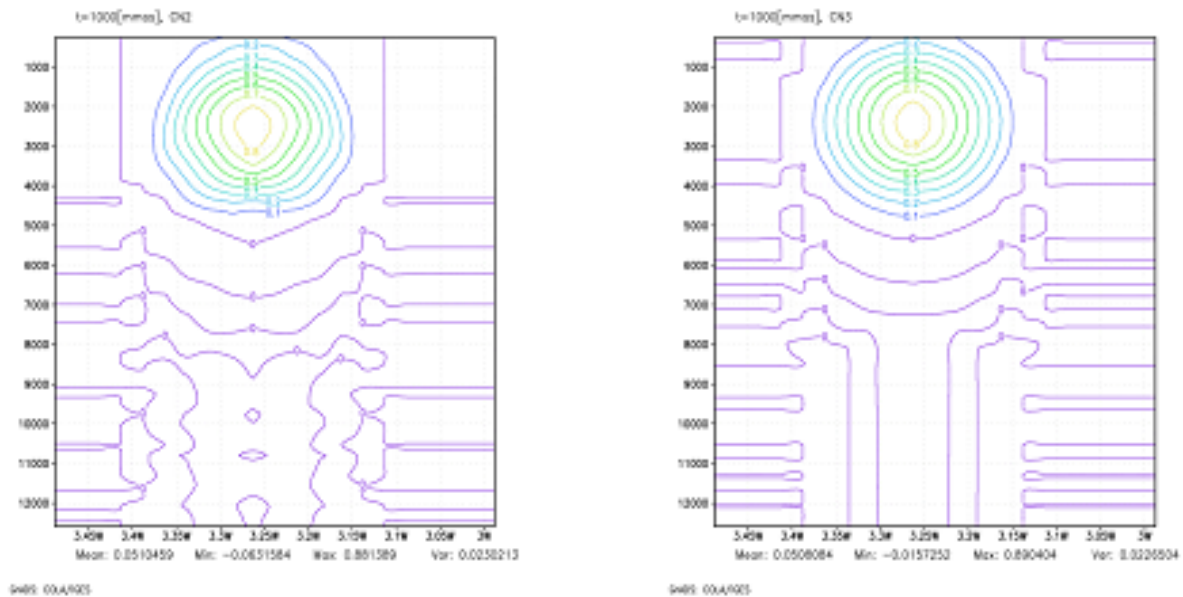
Figure 29: Implicit vertical advection; test with a constant velocity and starting with a cone distribution, 2nd order (left), 3rd order (right).

Not yet inspected is an alternative approach: the calculation of the vertical advection outside of the Runge-Kutta scheme. There are two reasons for that: first, the implicit advection needs no stabilization through the Runge-Kutta scheme, second, an implicit scheme is not very well suited for use in a Runge-Kutta substep. Questions of stability (in combination with the fast waves solver) and accuracy (splitting error) have to be inspected.

2.7.1   Addendum

Some months after finishing the Priority Project, the work on this task could be continued. The use of the implicit scheme outside of the RK-scheme leads to promising results. Pure 2D-advection tests show a strongly improved behaviour compared to the currently used scheme. The coupling with fast waves is stable and shows no significant splitting error as could be shown with linearized 2D shallow water equations. Beyond this, idealized and real test cases with the COSMO-model show a realistic behaviour of the new implicit scheme.

2.8   Task 9: Physics coupling scheme

A special procedure to couple microphysics and dynamics is described in the WRF documentation (Skamarock et al. 2005). A similar numerical treatment of latent heat is now implemented in the Runge-Kutta core of the COSMO-DE. In both models the microphysics parameterizations are calculated in one Eulerian time step after the Runge-Kutta integration of the dynamical core and the Marchuk-splitting method is used here to finally update the fields in a balanced way and complete the time step. The diabatic heating term in the prognostic equation for temperature includes the physical tendencies due to radiation, convection, turbulent mixing and latent heat conversion in the microphysics (e.g. the saturation adjustment). While the former tendencies are integrated within the acoustic steps, the last temperature tendency has not been part of this integration. The new variant uses the tendency due to latent heat conversion of the previous time step as an estimate which enters the integration of the fast waves in the same way than the other physical tendencies. After the Runge-Kutta update, this tendency estimate is subtracted again and the time step is completed as before. Tests with this new variant of coupling showed deficiencies especially in combination with the moist turbulence scheme. Especially vertical cross sections revealed $2\Delta z$-structures of the TKE and cloud water fields. To circumvent these problems the temperature tendencies in the saturation adjustment step directly after the Runge-Kutta integration do not enter the summation of the latent heat tendencies. This could only be a preliminary solution. The reason for the mentioned problems should be studied further. Also other possibilities for the physics-dynamics coupling should be investigated.

2.9   Task 10: Testing of alternative fast wave scheme

In Gassmann (2005) a new split-explicit time integration scheme was proposed. This scheme is alternative to the Wicker-Skamarock type (1998, 2002) of splitting, which is closely related to the Runge-Kutta (RK) method. According to Gassmann this splitting method seems to have a stable and smaller splitting error compared to other existing split explicit schemes based on RK. The Gassmann scheme seems to be also more sensitive to the inconsistencies in the fast-waves terms than the RK version of Wicker and Skamarock. According to Gassmann along with this splitting method it is necessary to use the non-isotropic divergence damping and to include the vertical p*/T advection terms related to the vertical velocity w to have a consistent fast-mode solver. This implies the splitting up of vertical p*/T advection into two parts related to the two components of the contravariant vertical velocity ζ:

$$\dot\zeta = \dot\xi - \frac{1}{\sqrt{G}}w| \tag{18}$$

where

$$\dot{\xi} = \frac{1}{\sqrt{G}}(\frac{u}{acos\varphi}\frac{\partial z}{\partial \lambda} + \frac{v\partial z}{a\partial \varphi})| \tag{19}$$

the first one responsible for the actual vertical advection placed in the fast-waves solver and the second one accounting for a vertical advection component apparently present because of terrain-following coordinates involved in the slow-mode equations. A direct application of the free-slip condition is no longer possible in the p*/T slow vertical advection terms of the pressure and temperature equations. At the lower boundary the advective part of the model determines the w field:

$$w_{lowbound} = (\frac{u}{acos\varphi}\frac{\partial z}{\partial \lambda} + \frac{v\partial z}{a\partial \varphi})_{lowbound} \tag{20}$$

According to Gassmann (2006) the lower BC in this form is a slow term and it should be evaluated once per large time step and thus been held constant during the short time integration. Actually, in the slow part the full ξ=0 at the lower boundary is used (instead of ζ) in the vertical p*/T advection to avoid the evaluation of a vertical p*/T gradient which was not available in the numerical grid. A COSMO model version including the new time splitting scheme and fast-waves solver along with its documentation (Gassmann, 2006) was provided by Almut Gassmann (at that time Uni Bonn). All the tests performed with this version of code were not successful. The COSMO model crashed after a few hours of integration. Preliminary tests using the Gassmann splitting method implemented using the fast-waves solver of the RK core (without the vertical p*/T advection splitting and with the isotropic divergence damping) was successful (unofficial code) showing similar results to the default Wicker-Skamarock type RK scheme (MSLP scores are showed in Fig. 30). The above described formulation of the lower boundary condition used for the vertical p*/T advection splitting could probably be responsible for these crashes, but the issue how to formulate an appropriate lower boundary condition in this case has not been addressed.
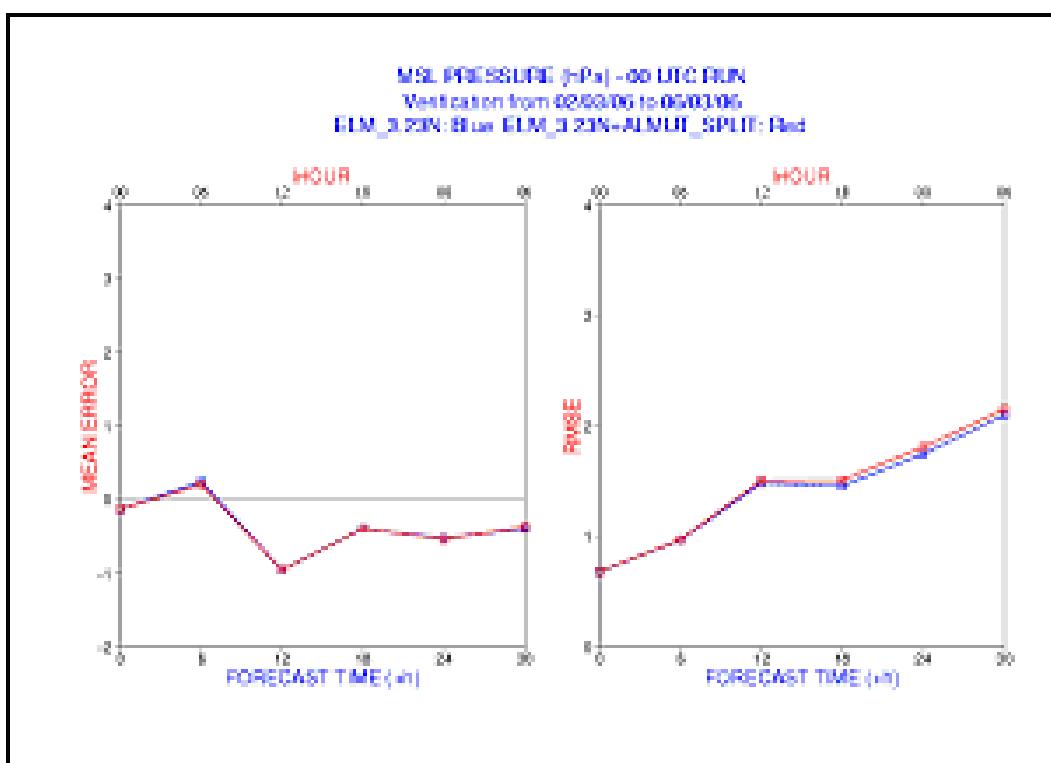
Figure 30: Comparison of pressure at MSL between the 'standard-RK' scheme and the 'Gassmann-RK'-scheme.

2.10   Task 13: Divergence damping in a true 3D-version

Cases occurred, where the up to now used 'quasi-2D' divergence filtering lead to unstable results. But a complete abandoning of the divergence filtering (as proposed by A. Gassmann for her dynamical core) also leads to several instabilities. This was also shown by stability analyzes of the RK-core by M. Baldauf. P. Prohl (DWD) could demonstrate that the Bryan-Fritsch-test case of a rising warm bubble is unstable with 'quasi-2D' divergence damping but becomes stable only with a full 3D (=isotropic) version (realized with a preliminary explicit formulation). For operational use an implicit version of 3D divergence damping is necessary. This task was defined relatively late and could not be treated during the project.

2.11   Task 14: Digital Filter Initialization (DFI)

DFI is an initialization scheme based on time filtering proposed by Lynch and McDonald (1990). The high frequencies are removed by applying a digital filter to a short time series of the prognostic model variables obtained by an integration from the initial data. The twice digital filter initialization (Lynch and Huang, 1994), implemented in COSMO model, consists of two model integrations subjected to a filter of span T: an adiabatic backward integration from 0 to -T and a diabatic forward integration from -T/2 to T/2 (see COSMO scientific documentation, part 1 for further details). The backward integration is realized by simply changing the time step Δt to $-\Delta t$. DFI did not work appropriately both in Leap-Frog (LF) and Runge-Kutta (RK) dynamical core. DFI using LF dynamics works correctly in COSMO model V3.23 with a 7 km grid spacing, after having fixed an error in the treatment of the boundary condition (dfi_initialization.f90). Some technical changes (mostly in the numerical functions of advection) were needed to run DFI using the RK core (dfi_initialization.f90, src_runge_kutta.f90, src_advection_rk.f90, fast_waves_rk.f90, numeric_utilities_rk.f90). All the odd order advection operators were changed to run in the backward model integration. The problem was that the odd order advection operators contain a dissipative term that needs a special treatment in the backward integration of the DFI. For example the 5th order horizontal advection operator is the sum of the 6th order advection operator and a dissipative term.

$$L_i^h(\phi)^{(5th)} = L_i^h(\phi)^{(6th)} + \frac{|u_i|}{60\Delta x}[-\phi_{i-3} + 6(\phi_{i-2} + \phi_{i+2}) - 15(\phi_{i-1} + \phi_{i+1}) + 20\phi_i - \phi_{i+3}] \quad (21)$$

The last term includes an absolute value of velocity and needs to be treated as the horizontal diffusion operator in the backward model run (sign of the diffusion coefficients reversed). The dissipative term of the odd order advection operators is multiplied to -1, when the integration time step is less than 0 (modifications in the next release of COSMO model). Additionally an optimization of the horizontal advection routines could be carried out by abandoning the concept of an operator acting on every grid point and using instead field operations, which can be much better optimized.

DFI using RK dynamics works well with a 7 km grid spacing after these changes. An example of the domain averaged surface pressure tendency and grid scale rain flux behaviours, as a function of the time step, are showed respectively in Fig. 31 and Fig. 32 for RK runs with (solid line) and without (dashed line) DFI. Some problems were found using RK core with a 2.8 km grid spacing. DFI worked only in some cases using the explicit version of the vertical advection.
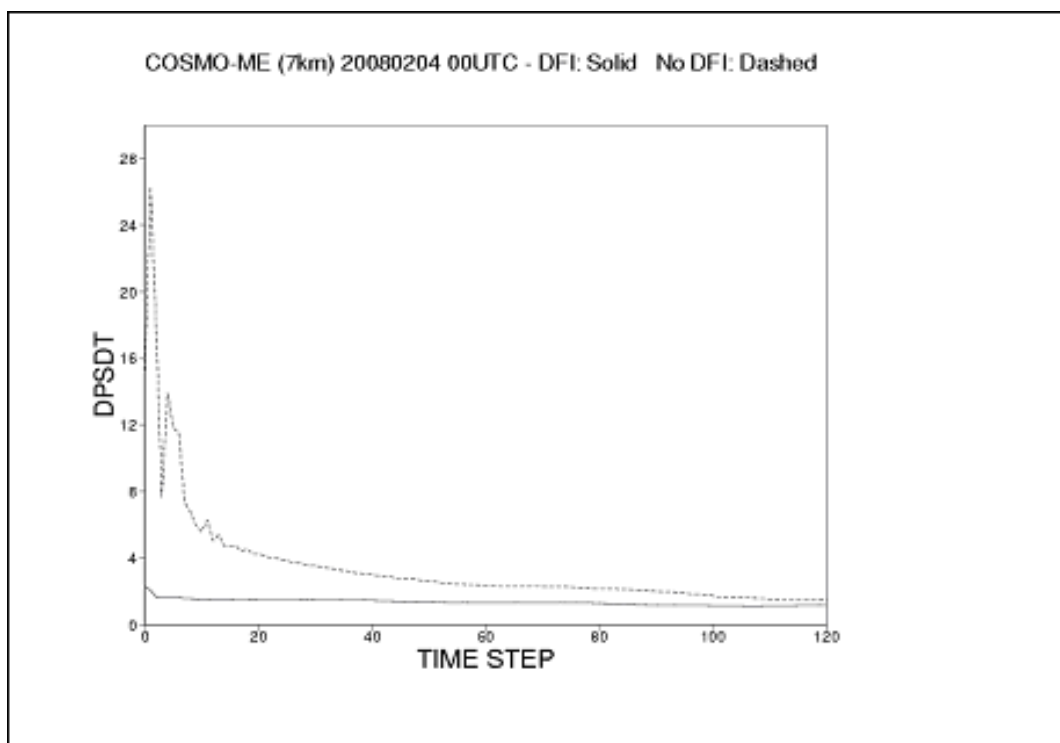
Figure 31: Domain averaged surface pressure tendency for a simulation with and without DFI.
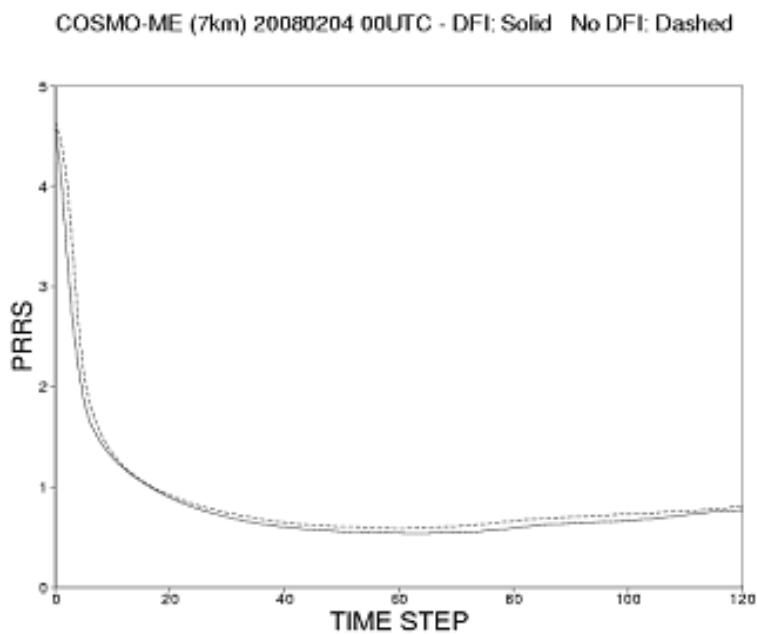
Figure 32: Grid scale rain flux for a simulation with and without DFI.

2.12   Open points

The Runge-Kutta scheme used here is adapted mainly from the WRF-model. The question that arises is if this basic scheme can be improved. A study about the stability of several combinations of Runge-Kutta schemes and horizontal advection schemes leads to only 3 useable combinations: namely RK3+upwind 3rd or 5th order and RK4 + centered difference 4th order (Baldauf, 2008a). This question was not yet inspected with the full COSMO model. Despite the fact that the pressure bias problem could be improved at least by the combination of several measures, the need of an at least mass conserving dynamical core is obvious. The problem of steep orography was solved by a slightly stronger filtering of the orography. Of course it would be more satisfying to solve this problem at the level of the discretization. Again, there is some hope to tackle this with a more conservative dynamical core (compare very interesting results with the EULAG model).

2.13   Resources used

0. Project leader	0.27
1. Looking at pressure bias	0.875
2. Continue RK case studies	0.623
3. Conservation	0.155
4. Advection of moisture quantities in conservation form	0.47
5. Investigation of convergence	0.775
6. Deep valleys	0.275
7. Different filter options for orography	0.05
8. Higher order discretization in the vertical	0.1
9. Physics coupling scheme	0.225
10. Testing of alternative fast wave scheme (Gassmann)	0.7
13. Divergence damping in a truly 3D-version	0
14. DFI corrections for RK	0.15
	sum= 4.668 FTE

2.14   Lessons learned

In this project people or rather small working groups from at least 4 different locations contributed to this project. Of course, it is not easy to communicate the relevant information among such different groups. During the project, the management instruments changed rather quickly (different forms of Excel-sheets, different web-based tools). During a project a more consistent reporting philosophy is certainly helpful. And, of course, only the most important reporting should be required.

3   Acknowledgements

List of contributing scientists during the whole project lifetime (in alphabetical order):

- Michael Baldauf (Deutscher Wetterdienst (DWD), Germany)

- Gabriella Ceci (Centro Italiano Ricerche Aerospaziali (CIRA), Italy)

- Jochen Förstner (Deutscher Wetterdienst (DWD), Germany)

- Oliver Fuhrer (MeteoSchweiz, Switzerland)

- Almut Gassmann (Max-Planck-Insitut, Hamburg, Germany)

- Hans-Joachim Herzog (Deutscher Wetterdienst (DWD), Germany)

- Guy de Morsier (MeteoSchweiz, Switzerland)

- Thorsten Reinhardt (Universität Köln, Germany)

- Gdaly Rivin (Federal Service for Hydrometeorology and Environmental Monitoring, Russia)

- Lucio Torrisi (Centro Nazionale di Meteorologia e Climatologia Aeronautica (CN-MCA), Italy)

- Pier Luigi Vitagliano (Centro Italiano Ricerche Aerospaziali (CIRA), Italy)

- Günther Zängl (Deutscher Wetterdienst (DWD), Germany)

4   References

M. Baldauf (2008a): Stability analysis for linear discretization of the advection equation with Runge-Kutta time integration, J. Comput. Phys. 227, 6638-6659.

M. Baldauf (2008b): A Tool for Testing Conservation Properties in the COSMO-Model . COSMO-Newsletter No. 7.

M. Baldauf (2008c): A linear solution for flow over mountains and its comparison with the COSMO model, COSMO-Newsletter No. 9.

A. Bott (1989): A Positive Definite Advection Scheme obtained by Nonlinear Renormalization of the Advective Fluxes, Mon. Wea. Rev. 117/5, 1006-1015.

J. Förstner, M. Baldauf, A. Seifert (2006), Courant Number Independent Advection of the Moisture Quantities for the LMK, COSMO-Newsletter No. 6.

A. Gassmann (2002): Numerische Verfahren in der nichthydrostatischen Modellierung und ihr Einfluss auf die Güte der Niederschlagsvorhersage, PhD-Thesis, Berichte des Deutschen Wetterdienstes, Offenbach.

A. Gassmann (2004): Formulation of the LM's dynamical lower boundary condition, COSMO-Newsletter No. 4.

A. Gassmann, H.-J. Herzog (2006): Internal report, DWD, Offenbach.

J. B. Klemp, R. B. Wilhelmson (1978): The Simulation of Three-Dimensional Convective Storm Dynamics, J. Atmos. Sci. 35, 1070-1096.

P. Lynch, A. McDonald, 1990: A multi-level limited area slow equation model: application to initialization. Q. J. Roy. Met. Soc., 116, 595-609.

P. Lynch, X.-Y. Huang, 1994: Diabatic initialization using recursive filters. Tellus, 46A, 583-597.

W. C. Skamarock, J. B. Klemp, J. Dudhia, D. O. Gill, D. M. Barker, W. Wang, J. G. Powers (2005): A Description of the Advanced Research WRF Version 2, NCAR Technical Note, NCAR, Boulder, Colorado, USA.

W. C. Skamarock (2006): Positive-definite and Monotonic Limiters for Unrestricted-Time-Step Transport Schemes, Mon. Wea. Rev. 134, 2241-2250.

L. Torrisi (2005): Impact of Domain Size on LM Forecast, COSMO-Newsletter No. 5.

M. L. Weisman, J. B. Klemp, (1982): The dependence on numerically simulated convective storms on vertical wind shear and buoyancy. Mon. Wea. Rev., 110, 504-520.

L. J. Wicker, W. C. Skamarock (1998): A Time-Splitting Scheme for the Elastic Equations incorporating Second-Order Runge-Kutta Time Differencing, Mon. Wea. Rev. 126, 1992-1999.

L. J. Wicker, W. C. Skamarock (2002): Time Splitting Methods for Elastic Models using Forward Time Schemes, Mon. Wea. Rev. 130, 2088-2097.

List of COSMO Newsletters and Technical Reports

(available for download from the COSMO Website: www.cosmo-model.org)

COSMO Newsletters

No. 1: February 2001.

No. 2: February 2002.

No. 3: February 2003.

No. 4: February 2004.

No. 5: April 2005.

No. 6: July 2006.

No. 7: April 2008; Proceedings from the 8th COSMO General Meeting in Bucharest, 2006.

No. 8: September 2008; Proceedings from the 9th COSMO General Meeting in Athens, 2007.

No. 9: December 2008.

COSMO Technical Reports

No. 1: Dmitrii Mironov and Matthias Raschendorfer (2001):
Evaluation of Empirical Parameters of the New LM Surface-Layer Parameterization Scheme. Results from Numerical Experiments Including the Soil Moisture Analysis.

No. 2: Reinhold Schrodin and Erdmann Heise (2001):
The Multi-Layer Version of the DWD Soil Model TERRA_LM.

No. 3: Günther Doms (2001):
A Scheme for Monotonic Numerical Diffusion in the LM.

No. 4: Hans-Joachim Herzog, Ursula Schubert, Gerd Vogel, Adelheid Fiedler and Roswitha Kirchner (2002):
LLM ¯ the High-Resolving Nonhydrostatic Simulation Model in the DWD-Project LIT-FASS.
Part I: Modelling Technique and Simulation Method.

No. 5: Jean-Marie Bettems (2002):
EUCOS Impact Study Using the Limited-Area Non-Hydrostatic NWP Model in Operational Use at MeteoSwiss.

No. 6: Heinz-Werner Bitzer and Jürgen Steppeler (2004):
Documentation of the Z-Coordinate Dynamical Core of LM.

No. 7: Hans-Joachim Herzog, Almut Gassmann (2005):
Lorenz- and Charney-Phillips vertical grid experimentation using a compressible nonhydrostatic toy-model relevant to the fast-mode part of the 'Lokal-Modell'

No. 8: Chiara Marsigli, Andrea Montani, Tiziana Paccagnella, Davide Sacchetti, André Walser,
Marco Arpagaus, Thomas Schumann (2005):
Evaluation of the Performance of the COSMO-LEPS System

No. 9: Erdmann Heise, Bodo Ritter, Reinhold Schrodin (2006):
Operational Implementation of the Multilayer Soil Model

No. 10: M.D. Tsyrulnikov (2007):
Is the particle filtering approach appropriate for meso-scale data assimilation ?

No. 11: Dmitrii V. Mironov (2008):
*Parameterization of Lakes in Numerical Weather Prediction. Description of a Lake
Model.*

No. 12: Adriano Raspanti (2009):
COSMO Priority Project "VERification System Unified Survey" (VERSUS): Final Report

No. 13: Chiara Marsigli (2009):
*COSMO Priority Project "Short Range Ensemble Prediction System" (SREPS): Final
Report*

No. 14: Michael Baldauf (2009):
*COSMO Priority Project "Further Developments of the Runge-Kutta Time Integration
Scheme" (RK): Final Report*

COSMO Technical Reports

Issues of the COSMO Technical Reports series are published by the *COnsortium for Small-scale MOdelling* at non-regular intervals. COSMO is a European group for numerical weather prediction with participating meteorological services from Germany (DWD, AWGeophys), Greece (HNMS), Italy (USAM, ARPA-SIMC, ARPA Piemonte), Switzerland (MeteoSwiss), Poland (IMGW) and Romania (NMA). The general goal is to develop, improve and maintain a non-hydrostatic limited area modelling system to be used for both operational and research applications by the members of COSMO. This system is initially based on the COSMO-Model (previously known as LM) of DWD with its corresponding data assimilation system.

The Technical Reports are intended

- for scientific contributions and a documentation of research activities,
- to present and discuss results obtained from the model system,
- to present and discuss verification results and interpretation methods,
- for a documentation of technical changes to the model system,
- to give an overview of new components of the model system.

The purpose of these reports is to communicate results, changes and progress related to the LM model system relatively fast within the COSMO consortium, and also to inform other NWP groups on our current research activities. In this way the discussion on a specific topic can be stimulated at an early stage. In order to publish a report very soon after the completion of the manuscript, we have decided to omit a thorough reviewing procedure and only a rough check is done by the editors and a third reviewer. We apologize for typographical and other errors or inconsistencies which may still be present.

At present, the Technical Reports are available for download from the COSMO web site (www.cosmo-model.org). If required, the member meteorological centres can produce hardcopies by their own for distribution within their service. All members of the consortium will be informed about new issues by email.

For any comments and questions, please contact the editors:

Massimo Milelli   Ulrich Schättler
Massimo.Milelli@arpa.piemonte.it   *Ulrich.Schaettler@dwd.de*